LITHOS 430-431 (2022) 106844

Contents lists available at ScienceDirect

LITHOS

journal homepage: www.elsevier.com/locate/lithos

Ancient crust-derived syenitic and A-type granitic intrusions in the Emeishan large igneous province, SW China

Gui-Wen Xu [a,b,c], Wei-Guang Zhu [a,*], Lan Chen [c], Hong Zhong [a,b], Yan-Jun Wang [d], Zhong-Jie Bai [a], Jun-Hua Yao [a], Peng-Cheng Hu [a]

[a] State Key Laboratory of Ore Deposit Geochemistry, Institute of Geochemistry, Chinese Academy of Sciences, 99 West Lincheng Road, Guiyang 550081, China
[b] University of Chinese Academy of Sciences, Beijing 100049, China
[c] College of Petroleum Engineering, Chongqing University of Science and Technology, Chongqing 401331, China
[d] State Key Laboratory of Nuclear Resources and Environment, East China University of Technology, Nanchang 330013, China

ARTICLE INFO

Keywords:
Zircon and baddeleyite U—Pb ages
Sr–Nd–O–Hf isotopes
Geochemistry
Syenites and A-type granites
Emeishan large igneous province
SW China

ABSTRACT

Within the inner zone of the Emeishan large igneous province (ELIP), SW China, there are several small syenitic and A-type granitic intrusions not spatially related to giant Fe–Ti–V-deposit-bearing mafic–ultramafic layered intrusions. The representative Heime syenitic and Huili granitic intrusions as well as their spatially associated mafic dykes were developed at ca. 260 Ma, contemporaneous with the ELIP. The Heime metaluminous syenites are K-rich and have moderate SiO_2 (60.1–61.4 wt%) and high total-alkali ($Na_2O + K_2O$ = 9.68–10.7 wt%) contents with high K_2O/Na_2O ratios (1.18 to 1.74). The Huili metaluminous granites are K-rich A-type granites with moderate–high SiO_2 (62.7–68.9 wt%), high total-alkali (7.96–8.62 wt%) and Zr (324–853 ppm) contents, and high 10,000 × Ga/Al ratios (2.68–3.22). Both of them are enriched in high-field-strength elements and light rare-earth elements, with significantly negative Nb–Ta–Sr–P–Ti anomalies. They also have highly evolved whole-rock Sr—Nd isotopic compositions (Heime syenites, $(^{87}Sr/^{86}Sr)_i$ = 0.7092–0.7105, $\varepsilon_{Nd}(t)$ = −7.77 to −6.09; Huili granites, $(^{87}Sr/^{86}Sr)_i$ = 0.7116–0.7146, $\varepsilon_{Nd}(t)$ = −6.34 to −5.32). Zircon $\delta^{18}O$ values of the Heime syenites (5.73‰–6.40‰) are slightly higher than those of the mantle zircons, and lower than those of the Huili granites (5.98‰–7.52‰). Zircon Hf 8isotopic compositions of the Huili granites ($\varepsilon_{Hf}(t)$ = −3.30 to +0.73) are higher than those of the Heime syenites ($\varepsilon_{Hf}(t)$ = −7.08 to −2.97), possibly indicating a more contribution of mantle component. In addition, the spatially associated mafic dykes display considerably higher $\varepsilon_{Nd}(t)$ values (Heime mafic dykes, −3.95 to −3.01; Heime mafic dykes, −0.58 to −0.51) than those of the Heime syenites and Huili granites.

The parental magmas of both the Heime syenites and the Huili A-type granites show a close affinity to the K-rich, metaluminous syenitic magmas. Based on the Sr–Nd–O–Hf isotopic compositions of the Heime syenites, Huili granites, and spatially associated mafic dykes, we suggest that the K-rich syenitic magmas parental to the Heime syenites were produced mainly by remelting of Paleo–Mesoproterozoic mafic meta-igneous rocks, whereas those parental to the Huili A-type granites were generated by the remelting of Paleo–Mesoproterozoic basement rocks and mixing with small amounts of coeval mantle-derived basaltic melts.

1. Introduction

The Permian Emeishan large igneous province (ELIP) of SW China represents a product of ca. 260 Ma mantle plume and crustal melting in the region (e.g., Chung et al., 1998; Chung and Jahn, 1995; He et al., 2003; Xiao et al., 2004; Xu et al., 2001, 2004). It is characterised by large volumes of continental flood basalts, with subordinate mafic–ultramafic and felsic (e.g., granites and syenites) intrusions and minor rhyolitic tuff (Shellnutt, 2014; Shellnutt and Zhou, 2007; Xu et al., 2001, 2008; Zhong et al., 2007, 2009, 2011; Zhou et al., 2002a, 2008).

Based on the crustal thickness estimates and differential seismic velocity layers, the ELIP can be divided into three roughly concentric zones (i.e. inner, intermediate and outer) (He et al., 2003; Xu et al., 2004). In the Panzhihua–Xichang (Pan–Xi) area of the inner zone of the ELIP (He et al., 2003; Xu et al., 2004), several relatively large syenitic and granitic plutons are temporally and spatially associated with the

* Corresponding author.
E-mail address: zhuweiguang@vip.gyig.ac.cn (W.-G. Zhu).

https://doi.org/10.1016/j.lithos.2022.106844
Received 8 January 2022; Received in revised form 16 August 2022; Accepted 17 August 2022
Available online 24 August 2022

large Fe–Ti–V oxide mineralized mafic–ultramafic layered intrusions. These granitic plutons can be further divided into I-type and A-type granites (Shellnutt et al., 2011; Shellnutt and Zhou, 2007; Zhong et al., 2007, 2009). The petrogenesis of the peraluminous I-type granites have been attributed to partial melting of the Yangtze Block basement rocks (i.e., old continental crust) due to injection of the Emeishan plume-related hot magmas (Shellnutt et al., 2011; Zhong et al., 2007, 2011; Zhu et al., 2017a). However, the origins of the metaluminous syenitic and peralkaline–metaluminous A-type granites remain debated (e.g., Shellnutt and Jahn, 2010; Shellnutt, 2014; Shellnutt and Zhou, 2008; Shellnutt et al., 2009a, 2009b, 2011; Shellnutt, 2014; Xu et al., 2008; Zhong et al., 2007, 2009, 2011). Several petrogenetic models have been proposed, including (1) fractionation of a common parental magma of layered gabbroic intrusions that host the giant Fe–Ti–V oxide deposits (Shellnutt and Jahn, 2010; Shellnutt and Zhou, 2007; Shellnutt et al., 2009b, 2011; Zhong et al., 2007, 2009, 2011, 2) partial melting of mafic juvenile crust (i.e., underplated mafic rocks) during Emeishan mantle plume (Shellnutt et al., 2009a; Shellnutt and Zhou, 2007, 2008; Xu et al., 2008), and (3) mixing between Emeishan basaltic magmas and crustal melts (Shellnutt, 2014; Shellnutt et al., 2011).

This study identified several small syenitic and A-type granitic intrusions within inner zone of ELIP. Unlike those large syenitic and

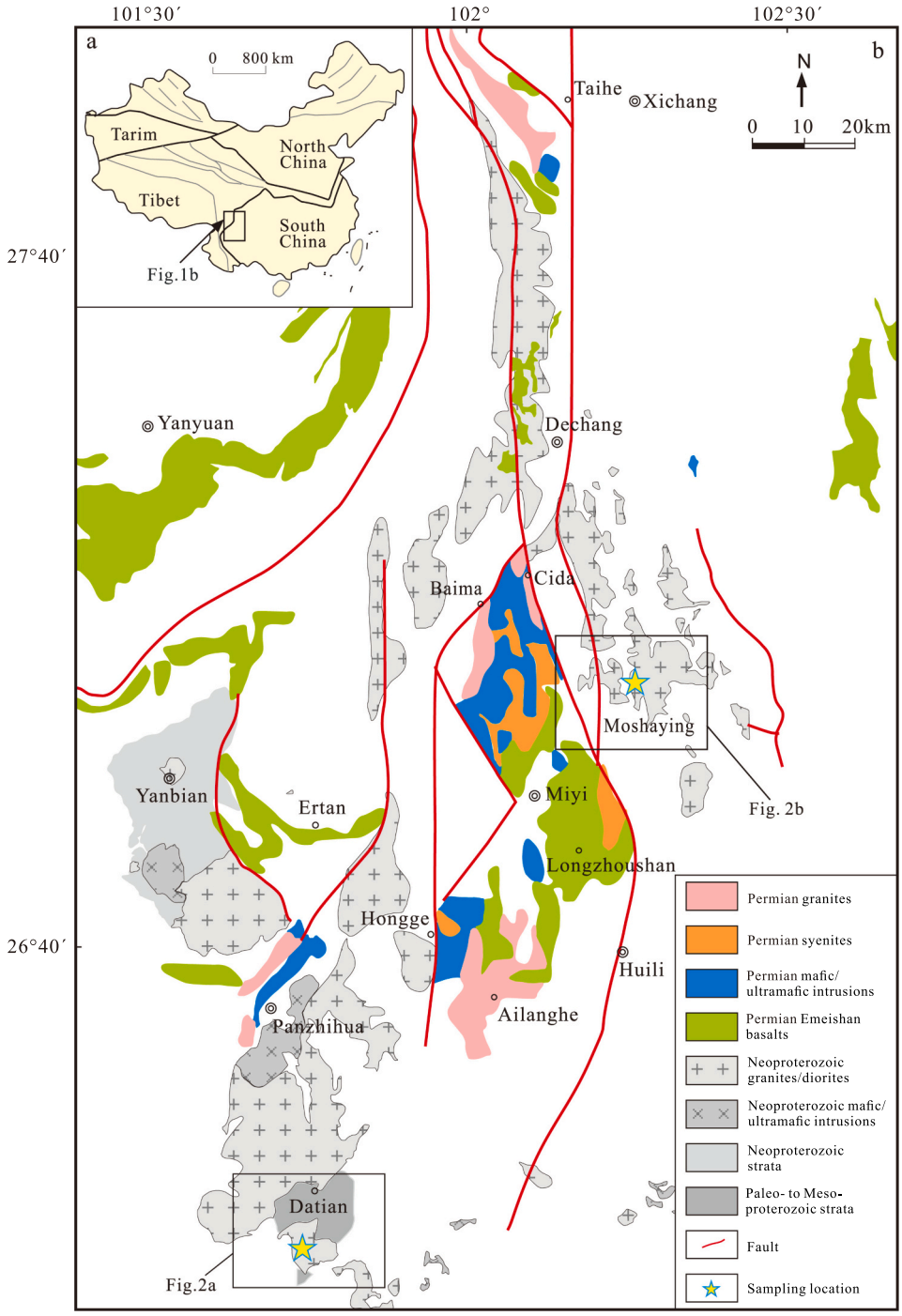

Fig. 1. (a) Simplified tectonic map showing the location of the Panzhihua–Xichang (Pan–Xi) area along the western margin of the Yangtze Block, SW China (modified from Zhong et al., 2007); (b) simplified geological map showing the distributions of Neoproterozoic and Permian intrusions in the Pan–Xi area (modified from the Sichuan 1:500,000 geological map; SBG, 1978; Zhong et al., 2007).

granitic plutons, these small intrusions are spatially far away from the giant Fe–Ti–V-deposit-bearing mafic–ultramafic layered intrusions. Therefore, these newly identified small syenitic and granitic intrusions may have a different origin from those of the previously reported large syenitic and granitic plutons, and consequently could provide unique information about the mantle-crust interaction during the formation of the ELIP. However, their origin has attracted little attention due to their small volumes. A recent study suggests that ancient granodiorite-like crustal material may have been highly involved into the genesis of some of the A-type granites within ELIP (Zhang et al., 2021), which cannot be explained by the above-mentioned models. If crust-derived syenites and A-type granites are identified within the inner zone of the ELIP, it will play an important role in understanding the new origin model of syenites and A-type granites in the region. Therefore, it deserves more effort to examine the role of ancient crust-derived silicic magmas during the formation of these syenites and A-type granites responding to the Emeishan plume thermal event.

Magmatic zircon Hf—O isotopic compositions can be used to trace the involvement of different source components and magma mixing (Griffin et al., 2002; Jeon et al., 2014; Kemp et al., 2007; Valley, 2003; Valley et al., 1998). Here we report zircon U—Pb ages and Hf—O isotopic compositions, and whole-rock elemental and Sr—Nd isotopic compositions of two newly discovered syenitic and A-type granitic intrusions in the Pan–Xi area. The aims of the study were to (1) determine crystallisation ages of the two syenitic and granitic intrusions, and (2) constrain the genetic link between the granites, syenites, and spatially associated mafic dykes. Our work highlights the role of the reworking of ancient crustal components and provides to a more complete scenario for multiple origins of syenites and A-type granites in response to the Permian plume thermal event in SW China.

2. Geological background and petrography

The late Permian (ca. 260 Ma) ELIP extends from SW China to NW Vietnam (Ali et al., 2005; Shellnutt, 2014). It covers an area of ~0.3 × 10^6 km^2 with a total thickness ranging from several hundred meters in the east (e.g., Guizhou Province) to 5000 m in the west (e.g., Yunnan Province) (Chung et al., 1998; Chung and Jahn, 1995; Shellnutt, 2014; Zhou et al., 2002a). The inner zone of the ELIP is located near the western margin of the Yangtze Block, SW China (Fig. 1a). The widespread basement in the western margin of the Yangtze Block comprises the late Paleoproterozoic Dahongshan, Hekou, Dongchuan, and Tong'an groups, which were intruded by 1.75–1.5 Ga mafic intrusions (Fig. 1a; Chen et al., 2013; Fan et al., 2020; Greentree and Li, 2008; Zhao et al., 2010; Zhu et al., 2017b). The Dongchuan–Kunyang and Tong'an–Huili groups consist of a sequence of greenschist facies meta-sedimentary and meta-volcanic rocks that likely developed at 1.75–1.0 Ga (Chen et al., 2013; Greentree and Li, 2008; Zhao et al., 2010; Zhu et al., 2016). These rocks are overlain by a thick (>9 km) sequence of Neoproterozoic (850–540 Ma) to Permian strata comprising clastic, carbonate, and metavolcanic rocks. In addition, Neoproterozoic magmatic rocks are widely distributed in the Pan–Xi area including granites, granodiorites, tonalites, mafic–ultramafic bodies, and mafic dykes (X. H. Li et al., 2003b; Z. X. Li et al., 2003a; Zhou et al., 2002b, 2006a, 2006b; Zhu et al., 2006, 2007, 2008).

The ELIP is characterised mainly by voluminous continental flood basalts, with subordinate mafic–ultramafic intrusions, syenites, and granites (Shellnutt, 2014; Xiao et al., 2004; Xu et al., 2001; Zhong et al., 2007, 2009, 2011; Zhou et al., 2008). The continental flood basalts are divided into two compositionally distinct groups, namely high-Ti (Ti /Y > 500) and low-Ti (Ti /Y < 500) basalts (Xiao et al., 2004; Xu et al., 2001). The Taihe, Baima, Hongge and Panzhihua complexes of mafic–ultramafic intrusions, granites, and syenites are mainly developed in the Pan–Xi area of the inner zone of the ELIP (Fig. 1b; Shellnutt and Jahn, 2010; Shellnutt and Zhou, 2007; Shellnutt, 2014; Shellnutt et al., 2009a, 2009b, 2011; Zhong et al., 2007, 2009, 2011; Zhou et al., 2008). Zircon U—Pb dating by laser ablation–inductively coupled plasma–mass spectrometry (LA–ICP–MS) and secondary ion mass spectrometry (SIMS) for the gabbros, syenites, and granites of these complexes indicates that the ages of felsic intrusive magmatism (256.2 ± 3.0 Ma to 259.8 ± 1.6 Ma) are indistinguishable from those of mafic intrusive magmatism (255.4 ± 3.1 Ma to 259.5 ± 2.7 Ma), and represent the final phase of a continuous magmatic episode spanning no >10 Myr (Zhong et al., 2011). In particular, the new chemical abrasion (CA)–thermal ionization mass spectrometry (TIMS) zircon U—Pb ages of the Huangcao, Daheishan, Woshui and Cida syenitic and granitic plutons and three mafic dykes in the Pan–Xi area are between >257 Ma and ca. 260 Ma (Shellnutt et al., 2012). In addition, the recent CA–isotope dilution (ID)–TIMS zircon U—Pb ages of the late-stage rhyolites and the neighboring silicic plutons from northern Vietnam are ~256.3–257.9 Ma (Shellnutt et al., 2020). These results suggest that ELIP magmatism lasted much <10 Myr.

Previous studies have shown that a number of large syenitic, and I-type and A-type granitic plutons in the Pan–Xi area are temporally and spatially associated with giant Fe–Ti–V-deposit-bearing mafic–ultramafic layered intrusions, which are closely related to the high-Ti basalts (Shellnutt, 2021; Shellnutt and Zhou, 2007; Zhong et al., 2007, 2009, 2011; Zhou et al., 2008). The Taihe syenitic and A-type granitic pluton is exposed along the Anning River–Yimen Fault and intrudes the western and southern parts of adjacent layered mafic–ultramafic intrusions (Xu et al., 2008; Zhong et al., 2011). It comprises mainly granite, quartz syenite, and amphibole-bearing syenite, and sensitive high-resolution ion microprobe (SHRIMP) zircon U—Pb age data indicate that it was emplaced at 261.4 ± 2.3 Ma (Xu et al., 2008). The Baima (including Cida–Huangcao) syenitic and A-type granitic pluton intruded the adjacent Baima layered mafic–ultramafic intrusion (Fig. 1b; Zhong et al., 2011). The Cida syenitic and A-type granitic pluton comprises mainly riebeckite granite and subordinate magnetite–biotite granite and quartz syenite, with alkaline syenite and amphibole syenite at its periphery. That pluton was previously dated at 256.2 ± 1.5 Ma by zircon LA–ICP–MS dating (Zhong et al., 2011) and 258.4 ± 0.6 Ma (Shellnutt et al., 2012) by zircon CA–TIMS U—Pb dating, respectively. The Huangcao syenitic pluton intruded gabbro in the upper zone of the Baima complex and has been dated at 258.9 ± 0.7 Ma by zircon CA–TIMS U—Pb dating (Shellnutt et al., 2012). The alkali feldspar syenite in the upper part of the Hongge mafic–ultramafic intrusion is comprised of ~90 vol% alkali feldspar and has been dated at 261.5 ± 2.4 Ma by zircon LA–ICP–MS technique (Shellnutt, 2021). The Ailanghe I-type granitic pluton intruded the Hongge mafic–ultramafic intrusion and adjacent Emeishan basalts, which comprise coarse–medium-grained biotite, K-feldspar granite, and medium–fine-grained monzonitic granite (Zhong et al., 2007). The Ailanghe granitic pluton was emplaced at 255.2 ± 3.6 Ma according to SHRIMP zircon U—Pb dating (Xu et al., 2008), and at 256.8 ± 2.8 Ma and 256.2 ± 3.0 Ma by the LA–ICP–MS technique (Zhong et al., 2011).

In contrast, some small felsic intrusions (e.g., Heime syenitic and Huili granitic intrusions) are not spatially associated from the large Fe–Ti–V oxide mineralized mafic–ultramafic layered intrusions. The Heime syenitic intrusion is circular in horizontal cross-section and is exposed over an area of ~2 km^2 (Figs. 1b and 2a). It intruded into the Neoproterozoic Datian granites and was cross-cut by mafic dykes (Figs. 2a and 3a). The rocks are scarlet and dark-grey in colour, fine– to medium-grained (Fig. 3b and c). These syenitic rocks comprise mainly subhedral K-feldspar (70–75 vol%), plagioclase (10–15 vol%), hornblende and augite (10–15 vol% combined), and accessory minerals including zircon, apatite, sphene and Fe—Ti oxides (Fig. 3d). Most K-feldspar and plagioclase, and some Fe—Mg minerals have undergone variable degrees of clayzation and chloritisation, respectively (Fig. 3d).

The Huili granitic intrusion is an elliptic intrusion and has an outcrop area of ~2.5 km^2 (Figs. 1b and 2b). It intruded into the Neoproterozoic Moshaying granitic pluton (790 ± 16 Ma; Guo et al., 2007; Fig. 2b) and was cross-cut by mafic dykes. The granites are red in colour, fine– to

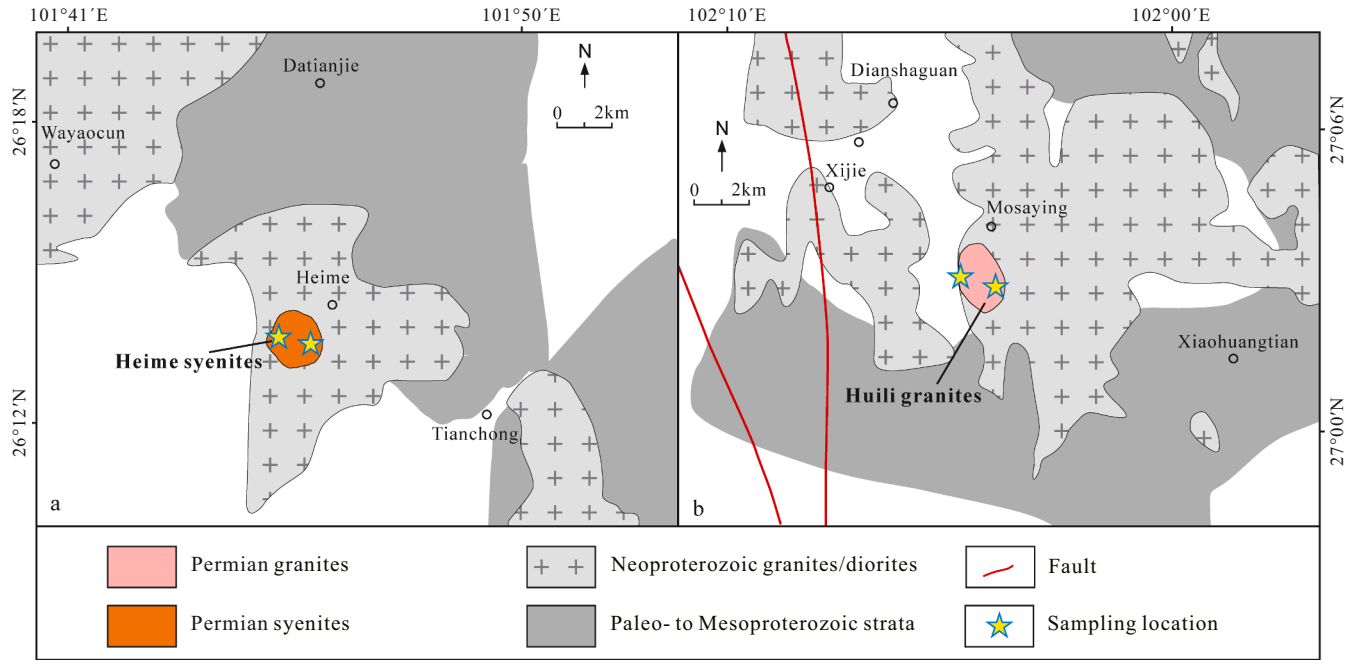

Fig. 2. Simplified geological map of (a) the Heime syenitic intrusion (modified after the Yongren 1:200,000 geological map; YBG, 1966) and (b) the Huili granitic intrusion (modified after the Miyi 1:200,000 geological map; SBG, 1966).

medium-grained, and comprise subhedral K-feldspar (60–65 vol%), plagioclase (20–25 vol%), quartz (20–25 vol%), and minor biotite and accessory minerals including zircon, apatite, and Fe—Ti oxides. Most K-feldspar and plagioclase underwent slight to moderate clayzation (Fig. 3f).

Mafic dykes intruding the Heime syenites and Huili granites are <2 m wide and grey-black in colour, and comprise mainly fine– to medium-grained plagioclase (50–60 vol%), clinopyroxene (30–35 vol%), biotite (5–10 vol%), and Fe—Ti oxides (5–10 vol%), with minor olivine (<5 vol %) and accessory minerals such as apatite.

3. Sampling and analytical methods

Thirty-six samples of the Heime syenite and related mafic dykes (28 and 8 samples, respectively), and twenty-six samples of the Huili granite and related mafic dykes (22 and 4 samples, respectively) were collected in this study (Fig. 2).

Zircon grains were separated from two samples of the Heme syenites (HM1401 and HM1519) and two samples of the Huili granites (HL1101 and HL1504), and baddeleyite grains were separated from one sample of the Huili mafic dykes (sample HL1703), using conventional heavy-liquid and magnetic techniques, and hand-picked under a binocular microscope. Zircon and baddeleyite grains were mounted in epoxy resin, polished, and coated with gold. Cathodoluminescence (CL) images and transmitted- and reflected-light photomicrographs were taken to show internal structures. Zircon U—Pb dating of samples HM1401 and HL1101 and baddeleyite U—Pb dating of sample HL1703 was carried out by a Cameca IMS-1280 SIMS microprobe at the Institute of Geology and Geophysics, Chinese Academy of Sciences (IGGCAS), Beijing, China, following the procedures described by Li et al. (2009). Zircon U—Pb zircon dating of samples HM1519 and HL1504 was undertaken by LA–ICP–MS at the State Key Laboratory of Ore Deposit Geochemistry, Institute of Geochemistry, Chinese Academy of Sciences (IGCAS), Guiyang, China, using the analytical settings and data processing procedures described by He et al. (2013).

Zircon oxygen isotope compositions of samples HM1401 and HL1101 were also determined by the Cameca IMS–1280 SIMS at the IGGCAS. The analytical procedure and operating conditions are similar to those described by Li et al. (2009, 2013). The Qinghu zircon standard was analysed together with unknowns, yielding a mean $\delta^{18}O = 5.5 \pm 0.2‰$ (2SE), indistinguishable from the recommended value of 5.4 ± 0.2‰ (2SE) (Li et al., 2013). In situ zircon Lu—Hf isotopic analyses involved a Neptune Plus (ThermoFisher Scientific, USA) MC–ICP–MS with a GeoLas 2005 LA system at the State Key Laboratory of Geological Processes and Mineral Resources, China University of Geosciences, Wuhan, China, with operating conditions and data acquisition methods similar to those described by Hu et al. (2012).

Whole-rock major-element compositions were determined using X-ray fluorescence (XRF) at ALS Chemex, Guangzhou, China, using certified reference materials NIM-GBW07105, GBW07163, GBM908–10, and MRGeo08 as standards. Analytical precision was better than 5%. Whole-rock trace-element compositions were determined using a PerkinElmer (USA) Sciex ELAN DRC-e ICP–MS at the State Key Laboratory of Ore Deposit Geochemistry, IGCAS. Powdered samples (50 mg) were digested in a 1:1 mixture of HF + HNO_3 in high-pressure Teflon-coated bombs at ~190 °C for 48 h (Qi et al., 2000). Rh was used as an internal standard to monitor signal drift during measurement. International standards GBPG-1 and OU-6, and Chinese National standards GSR-1 and GSR-3 were used for analytical quality control. Analytical precision was generally better than 10% for trace elements.

Dried powered samples for Sr—Nd isotopic analysis were dissolved in a 1:2:0.3 acidic mixture of HF, HNO_3, and $HClO_4$ in Teflon-coated bombs. Sr and Nd were separated by conventional cation-exchange chromatography. The Sr—Nd isotopic ratios were determined using a Micromass Isoprobe (Isotopx, UK) MC–ICP–MS at the State Key Laboratory of Environmental Geochemistry, IGCAS. The $^{87}Sr/^{86}Sr$ ratios were corrected for mass fractionation based on $^{86}Sr/^{88}Sr = 0.1194$, and $^{143}Nd/^{144}Nd$ ratios based on $^{146}Nd/^{144}Nd = 0.7219$. The $^{87}Sr/^{86}Sr$ ratio determined for the SRM987 Sr standard was 0.710250 ± 7 (2σ); $^{143}Nd/^{144}Nd$ ratios determined for the US Geological Survey standard BCR-2 and JNDI-1 Nd standards were 0.512629 ± 16 (2σ) and 0.512119 ± 14 (2σ), respectively. These values are consistent with the recommended values.

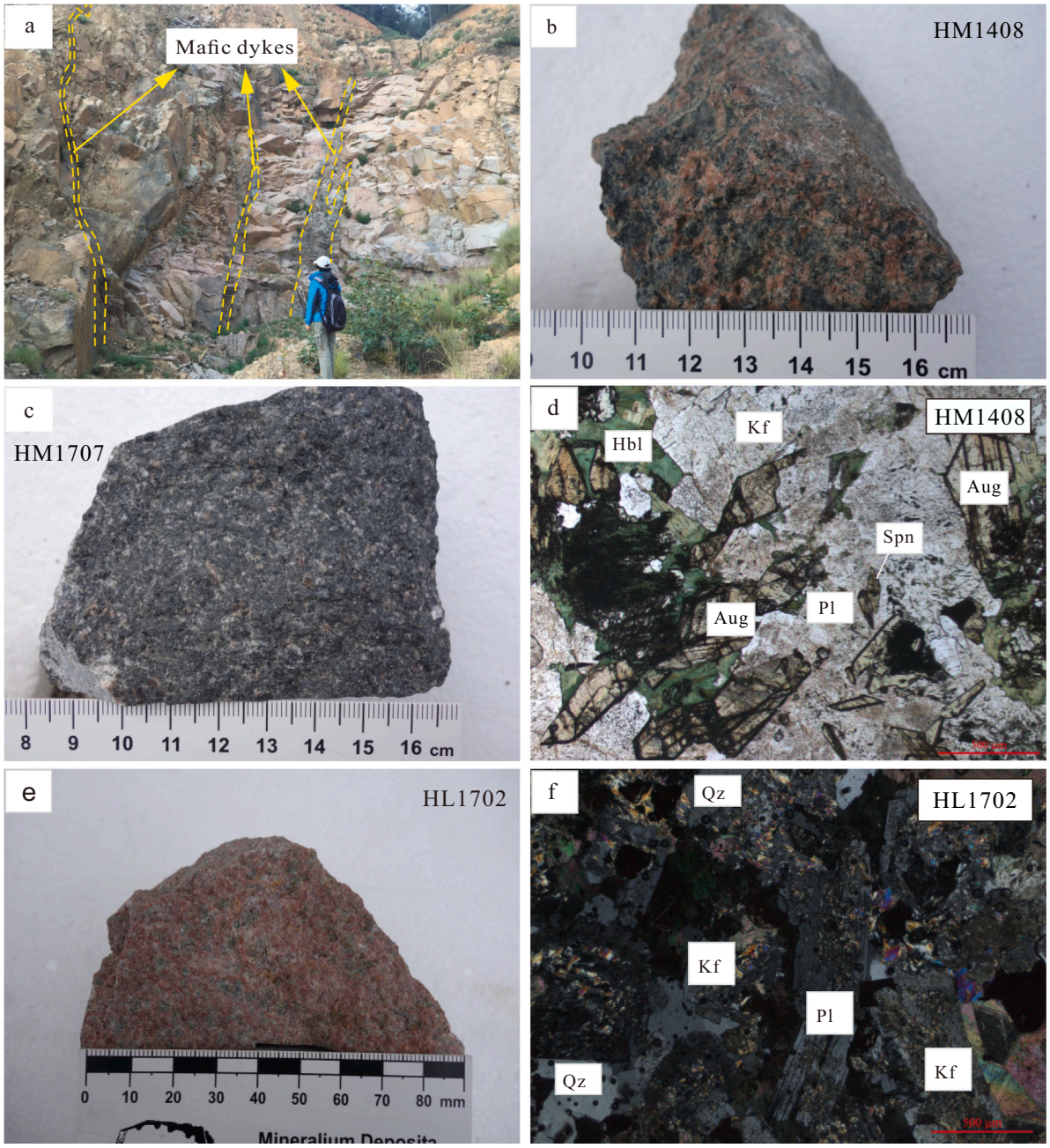

Fig. 3. Field photograph, hand specimen and microscopic photographs of the Heime syenites (a–d) and Huili granites (e, f). Kf, K-feldspar; Pl, plagioclase; Hbl, hornblende; Aug, augite; Mag, magnetite; Qz, quartz; Spn, sphene.

4. Results

4.1. Zircon and baddeleyite textures, trace elements and U—Pb ages

4.1.1. Heime syenites

Zircons from sample HM1401 are euhedral, 80–150 μm long, and have aspect ratios of 1.0–1.5. Most are prismatic crystals that show oscillatory zoning in CL images (Fig. 4a–d). The 17 analysed grains have U and Th contents and Th/U ratios of 93–203 ppm, 99–269 ppm, and 1.07–1.71, respectively (Table S1). The zircons are concordant in U—Pb and Pb—Pb isotopes within analytical error (Fig. 5a), with a concordia $^{206}Pb/^{238}U$ age of 259.9 ± 1.9 Ma (2σ; MSWD = 4.2), representing the crystallisation age of the sample.

Most zircons from sample HM1519 are euhedral and prismatic with obvious oscillatory zoning in CL images, and they have lengths of 60–150 μm and aspect ratios of 1–2 (Fig. 4e–h). LA–ICP–MS analysis of 19 zircons yielded U and Th contents and Th/U ratios of 134–232 ppm, 181–413 ppm, and 1.22–1.93, respectively (Table S2). The zircons are concordant in U—Pb and Pb—Pb isotopes within analytical error, with a concordia $^{206}Pb/^{238}U$ age of 259.8 ± 2.7 Ma (2σ, MSWD = 4.2; Fig. 5b), representing the crystallisation age of the sample.

4.1.2. Huili granites

Zircons from sample HL1101 are generally clear, euhedral, and prismatic, with distinct euhedral concentric zoning in CL images, and they have lengths of 60–100 μm and aspect ratios of 1–3 (Fig. 4i–l). SIMS analysis of 21 grains yielded U and Th contents and Th/U ratios of 74–268 ppm, 66–269 ppm, and 0.63–1.20, respectively (Table S1). The zircons are concordant in U—Pb and Pb—Pb isotopes within analytical error (Fig. 5c) and yield a $^{206}Pb/^{238}U$ age of 259.4 ± 1.2 Ma (2σ; MSWD

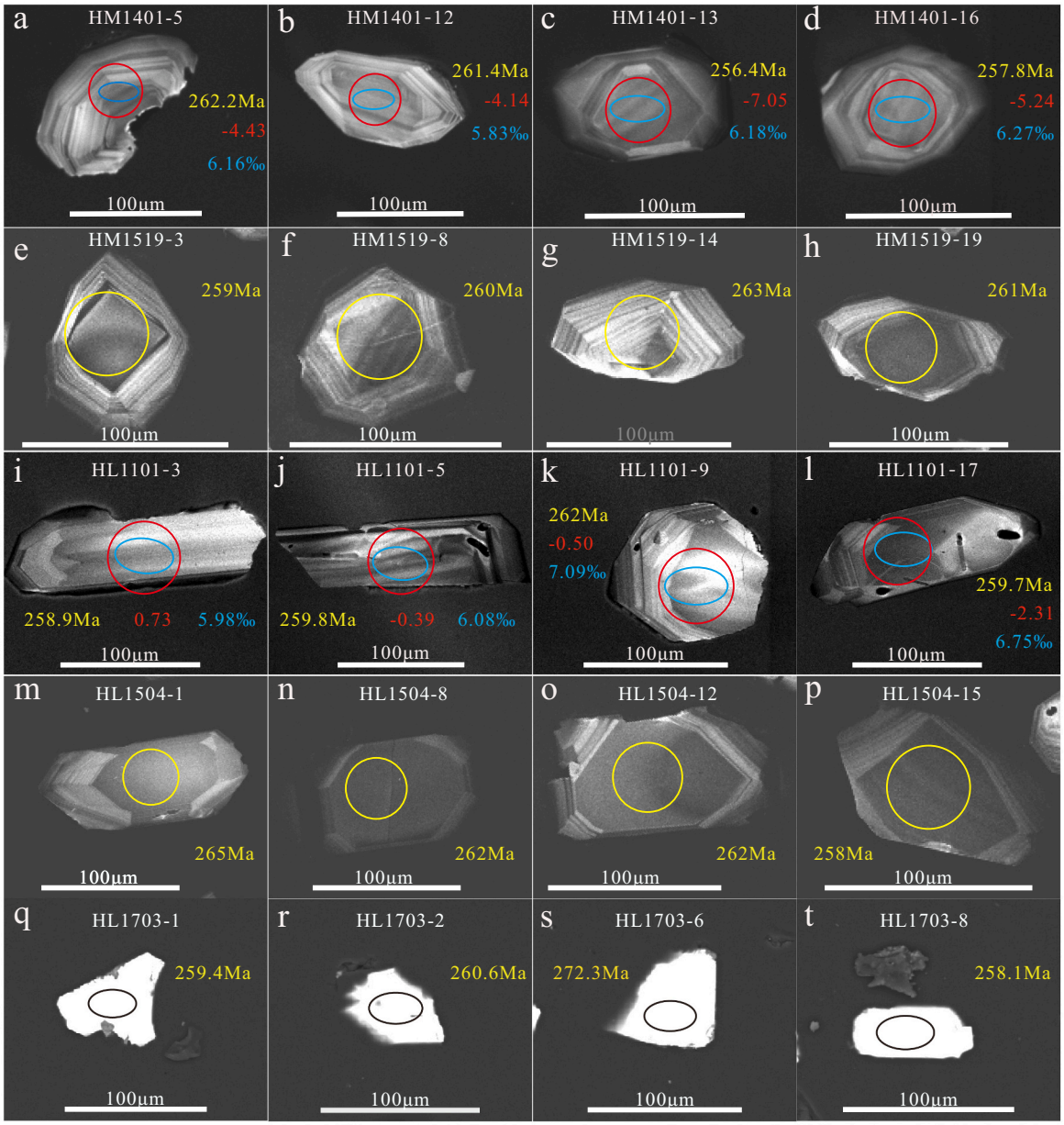

Fig. 4. Representative cathodoluminescence (CL) images of zircons from the Heime syenites (a–h) and Huili granites (i–p), and backscattered-electron images of baddeleyites from the Huili mafic dykes (q–t). Blue ellipses indicate SIMS spots for U—Pb and O isotopic analyses; red circles LA–ICP–MS Hf isotopic analyses; yellow circles LA–ICP–MS U—Pb analyses; black ellipses baddeleyite U—Pb analyses; yellow, red, and blue numbers represent U—Pb ages, $\varepsilon_{Hf}(t)$, and $\delta^{18}O$ values, respectively. (For interpretation of the references to colour in this figure legend, the reader is referred to the web version of this article.)

= 2.6), representing the crystallisation age of the sample.

Zircon grains from sample HL1504 are clear, euhedral, and prismatic crystals with distinct euhedral concentric zoning in CL images, and they have lengths of 50–120 μm and aspect ratios of 1–2 (Fig. 4m–p). LA–ICP–MS analysis of 18 grains yielded U and Th contents and Th/U ratios of 92–270 ppm, 69–280 ppm, and 0.64–1.04, respectively (Table S2). The zircons are concordant in U—Pb and Pb—Pb isotopes within analytical error, with a concordia $^{206}Pb/^{238}U$ age of 260.9 ± 2.8 Ma (2σ; MSWD = 0.01), representing the crystallisation age of the sample (Fig. 5d).

4.1.3. Huili mafic dykes

Most baddeleyite grains from sample HL1703 are subhedral, 30–80 μm in length, and have aspect ratios of 1–2 (Fig. 4q–t). Seventeen grains were analysed in a single analytical session, yielding U and Th contents and U/Th ratios of 450–1648 ppm, 5–53 ppm, and 0.005–0.061, respectively (Table S3). Nine grains are concordant in U—Pb and Pb—Pb isotopes within analytical error, yielding a concordia $^{206}Pb/^{238}U$ age of 260.8 ± 3.6 Ma (2σ; MSWD = 0.008) (Fig. 6; Table S3). This age is considered as the best estimate of the crystallisation age of the sample, and is interpreted as being the intrusive age of the mafic dykes.

Although field investigations show that the mafic dykes intrude the Huili granitic intrusion, zircon U—Pb dating results for the Heime syenites, Huili granites, and baddeleyite from the Huili mafic dykes suggest that the studied syenites and granites and mafic dykes were formed at ca. 260 Ma and almost synchronously (within analytical uncertainties).

4.2. Zircon Hf—O isotopes

Thirty-eight spot analyses of samples HM1401 and HM1519 from the Heime syenitic intrusion, and 35 spot analyses of samples HL1101 and HL1504 from the Huili granitic intrusion were undertaken for Hf

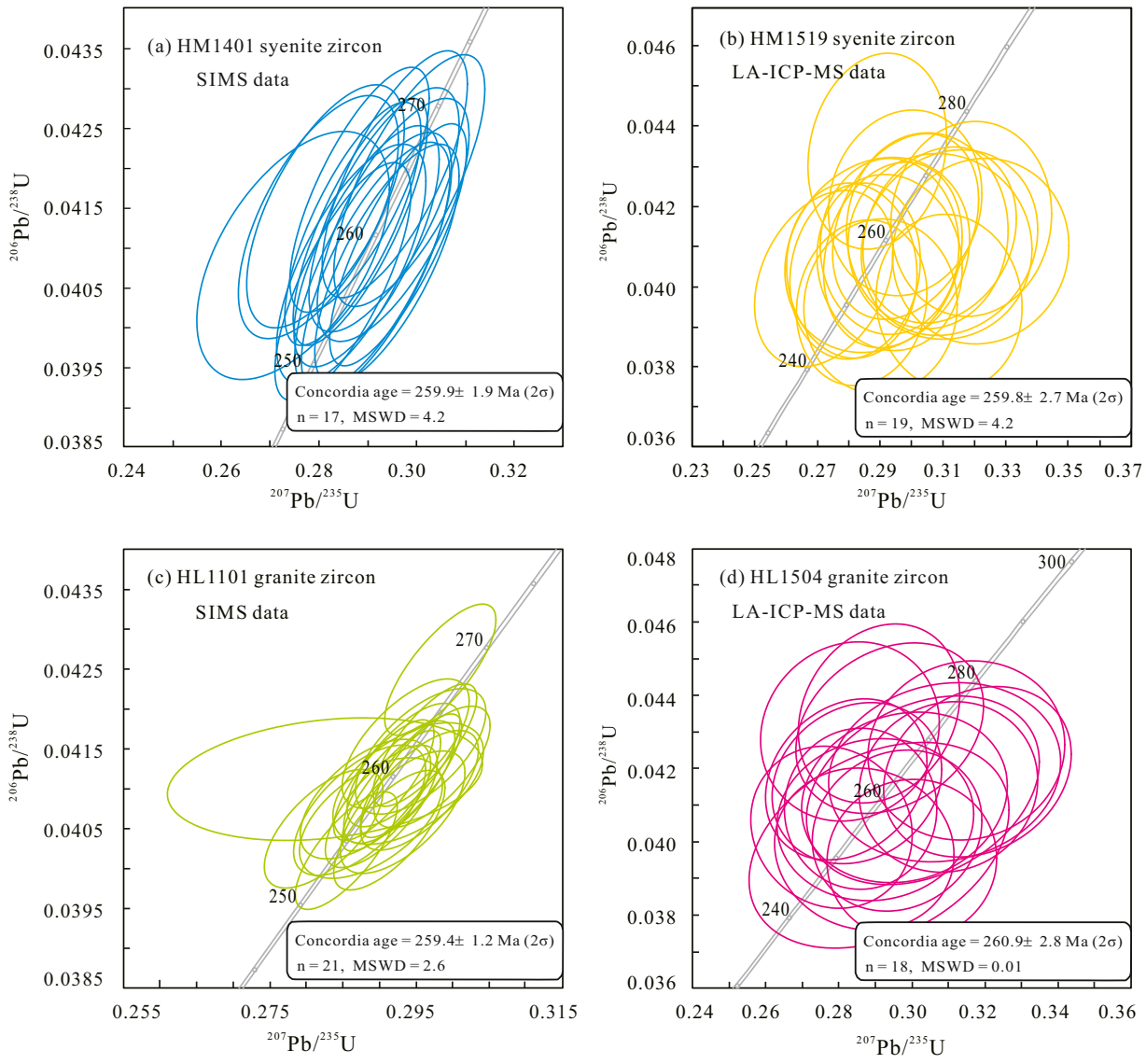

Fig. 5. U—Pb concordia diagrams of zircons from the Heime syenites (a, b; SIMS and LA–ICP–MS, respectively) and Huili granites (c, d; SIMS and LA–ICP–MS, respectively).

isotopes (Table S4; Fig. 7). Zircons from the Heime syenites have $\varepsilon_{Hf}(t)$ values of −7.08 to −2.97 and yield two-stage Hf model ages (T^{Hf}_{2MD}) of 1726–1423 Ma; zircons from the Huili granite have $\varepsilon_{Hf}(t)$ values of −3.30 to 0.73 and yield T^{Hf}_{2MD} ages of 1489–1229 Ma (Table S4; Fig. 7).

Zircon O isotopic compositions of sample HM1401 from the Heime syenite and sample HL1101 from the Huili granite are listed in Table S4. Zircons from the Heime syenite have slightly higher $\delta^{18}O$ values (5.73‰–6.40‰) than those of mantle (5.3‰ ± 0.3‰; Fig. 7b; Valley et al., 1998). The $\delta^{18}O$ values of zircons from the Huili granite are in the range 5.98‰–7.52‰, with most being higher than those of the Heime syenite and Ailanghe I-type granite ($\delta^{18}O$ = 7.2‰; unpublished data; Fig. 7b).

4.3. Whole-rock major and trace elements

Whole-rock major- and trace-element compositions of the Heime syenitic and Huili granitic intrusions, and spatially associated mafic dykes are listed in Table S5. All of the studied syenite and granite samples are fresh in hand sample, but variable degrees of alteration was found in the thin section, consistent with their variable and moderate loss on ignition (LOI) values (Heime syenites: 1.1–6.3 wt%; Huili granites: 1.2–5.1 wt%) (Table S5). To be conservative, major-oxide contents are corrected on a volatile-free basis, and only the major and trace elements that are negligibly affected by alteration (see section 5.1) will be utilized for the following results and further discussion.

4.3.1. Heime syenites and Huili granites

The Heime syenites have moderate SiO_2 contents (60.1–61.4 wt%; volatile-free); and high MgO (1.30–1.74 wt%), TiO_2 (1.14–1.33 wt%), Al_2O_3 (17.3–17.6 wt%), CaO (2.87–3.52 wt%), Na_2O (3.80–4.61 wt%), K_2O (5.46–6.78 wt%), and P_2O_5 (0.32–0.35 wt%) contents; and relatively low total iron (Fe_2O_3) contents (5.06–5.64 wt%) (Fig. 8). The MgO, Fe_2O_3, TiO_2, Al_2O_3, and K_2O contents of the Heime syenites exhibit slight decrease with increasing SiO_2, while the CaO, Na_2O, and P_2O_5 contents exhibit fairly constant (Fig. 8). Although their TiO_2, CaO and P_2O_5 contents are similar to those of the Panzhihua syenites at given SiO_2 contents, they have relatively higher MgO, Al_2O_3, and K_2O contents and lower Fe_2O_3 and Na_2O contents than the Panzhihua syenites (Fig. 8; Zhong et al., 2009). The Heime syenite samples have high total-alkali contents ($Na_2O + K_2O$ = 9.68–10.7 wt%) with high K_2O/Na_2O ratios (1.18 to 1.74) (Table S5; Figs. 8 and 9a). In the total-alkali–silica (TAS) diagram, the samples are plotted in the alkaline syenite and syenodiorite

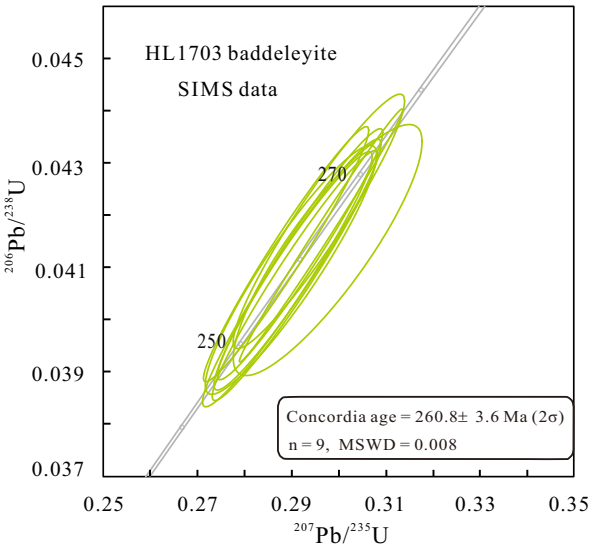

Fig. 6. Baddeleyite U—Pb concordia diagrams for the Huili mafic dykes that intrude the Huili granites.

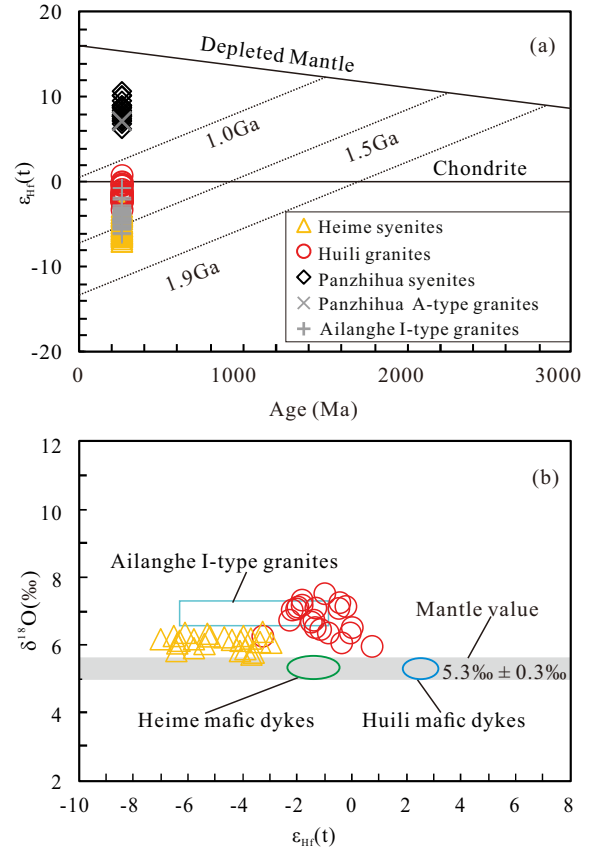

Fig. 7. Plots of zircon ε_{Hf} values vs. U—Pb ages (a) and zircon $\delta^{18}O$ values vs. ε_{Hf} values (b) of the Heime syenites and Huili granites. Zircon ε_{Hf} values for the Panzhihua syenites and granites, and Ailanghe I-type granites are from Zhong et al. (2009, 2011). Zircon $\delta^{18}O$ values of the Ailanghe I-type granites are unpublished data of the authors. The ε_{Hf} values for the Heime and Huili mafic dykes were calculated assuming $\varepsilon_{Hf} = 1.33\varepsilon_{Nd} + 3.19$ (Vervoort et al., 1999). The $\delta^{18}O$ values for the mafic dykes are similar to mantle $\delta^{18}O$ values (+5.3 ± 0.3‰; Valley et al., 1998).

fields (Fig. 9a). Their $Al_2O_3/(Na_2O + K_2O)$ (A/NK) and $Al_2O_3/(CaO + Na_2O + K_2O)$ (A/CNK) ratios are from 1.27 to 1.37 and from 0.89 to 0.95, respectively, indicating an affinity of metaluminous rocks (Table S5; Fig. 9b). Furthermore, all samples plot in the shoshonite field in the K_2O–SiO_2 diagram (Fig. 9c). In addition, their $FeO^T/(FeO^T + MgO)$ ratios range from 0.74 to 0.78, within the field of the ferroan (A-type) granites (Fig. 10a).

The Huili granites are characterised by moderate–high SiO_2 (62.7–68.9 wt%; volatile-free) and high total-alkali (Na_2O = 3.01–3.99 wt%; K_2O = 4.30–5.47 wt%; $Na_2O + K_2O$ = 7.96–8.62 wt%) contents with high K_2O/Na_2O ratios (1.08–1.81) (Table S5; Figs. 8 and 9a). The contents of other major oxides are variable: MgO, 0.66–1.79 wt%; Fe_2O_3, 4.02–5.98 wt%; TiO_2, 0.75–1.30 wt%; Al_2O_3, 14.4–16.6 wt%; CaO,2.23–3.50 wt%, and P_2O_5, 0.16–0.34 wt% (Table S5; Fig. 8). In Harker diagrams (Fig. 8), the MgO, Fe_2O_3, TiO_2, Al_2O_3, CaO, Na_2O, and P_2O_5 contents of the Huili granites decrease while the K_2O content increases with increasing SiO_2 content. Compared with the Panzhihua A-type granites, the Huili granites have relatively higher MgO, TiO_2, Al_2O_3, CaO, K_2O, and P_2O_5 contents, and lower SiO_2, $Fe_2O_3^T$, and Na_2O contents (Fig. 8; Zhong et al., 2009). In the TAS diagram (Fig. 9a), the samples are plotted in the alkaline syenodiorite to granite fields. Their A/NK ratios range between 1.31 and 1.49, and A/CNK ratios between 0.92 and 0.99 (Table S5). In the A/CNK versus A/NK diagram (Fig. 9b), they plot in the metaluminous granite field. In the K_2O versus SiO_2 diagram (Fig. 9c), these rocks plot in the field of the shoshonitic series. The Huili granites also display high $FeO^T/(FeO^T + MgO)$ ratios (0.72 to 0.85) and are plotted in the ferroan (A-type) granites (Fig. 10a).

The Heime syenites are enriched in total REE (ΣREE) contents (436–668 ppm) and light REEs (LREEs; 415–635 ppm) with $(La/Yb)_N$ ratios of 22.3–34.2 (the subscript N denotes chondrite-normalized; Boynton, 1984). Compared with the Panzhihua syenites, the Heime syenites have higher LREE contents and lower heavy REE (HREE) contents, with weakly negative Eu anomalies (Eu/Eu* = 0.76–0.96), while the Panzhihua syenites have strongly positive Eu anomalies (Fig. 11a; Zhong et al., 2009). The Heime syenites are enriched in high-field-strength elements (HFSEs) and depleted in Nb–Ta–Sr–P–Ti in the primitive-mantle-normalized multi-element diagram (Fig. 11b). Furthermore, all samples have high Ga (20.5–24.9 ppm), Zr (362–572 ppm), Nb (61.0–78.7 ppm), and Y (25.1–45.7 ppm) contents (Table S5). The 10,000 × Ga/Al ratios of the Heme syenites range from 2.36 to 2.68. On the basis of the Zr versus (10,000 × Ga/Al) diagram (Fig. 10b), these rocks are collectively plotted in the field of the A-type granitoids (Whalen et al., 1987).

The Huili granites have high ΣREE contents of 376–537 ppm with highly LREE-enriched. Compared with the Panzhihua A-type granites, the Heime granites show relatively lower REE contents with more obviously differentiated LREE and HREE patterns ($(La/Yb)_N$ = 15.4–21.8; Fig. 11c; Boynton, 1984). They have weakly negative anomalies (Eu/Eu* = 0.74–0.98), except for samples HL1511 and HL1512 which show weakly positive Eu anomalies. In the primitive-mantle-normalized incompatible-element diagram (Sun and McDonough, 1989), they appear significantly enriched in Th, La, Ce, Nd, and Zr, and depleted in Nb, Ta, Sr, P, and Ti (Fig. 11d). These rocks also have high Ga (19.7–25.6 ppm), Nb (33.2–74.2 ppm), Zr (324–853 ppm), and Y (36.9–50.1 ppm) contents (Table S5), and relatively high (Zr + Nb + Ce + Y) contents of 554–1129 ppm and 10,000 × Ga/Al ratios (2.68–3.22), similar to those of global-average A-type granites ((Zr + Nb + Ce + Y) > 350 ppm; 10,000 × Ga/Al = 3.75; Whalen et al., 1987). In the Zr versus (10,000 × Ga/Al) diagram all samples plot in the A-type granite field (Fig. 10b; Whalen et al., 1987).

Zirconium contents of the Heme syenites and Huili granites decrease with increasing SiO_2 content (Fig. S2a), suggesting that Zr concentrations in the evolving magma had already reached saturation. Magma temperatures can be estimated from zircon saturation temperatures (Boehnke et al., 2013). The calculated zircon saturation temperatures (T_{Zr}) for the Heme syenites are from 764 °C to 814 °C (Table S5) and

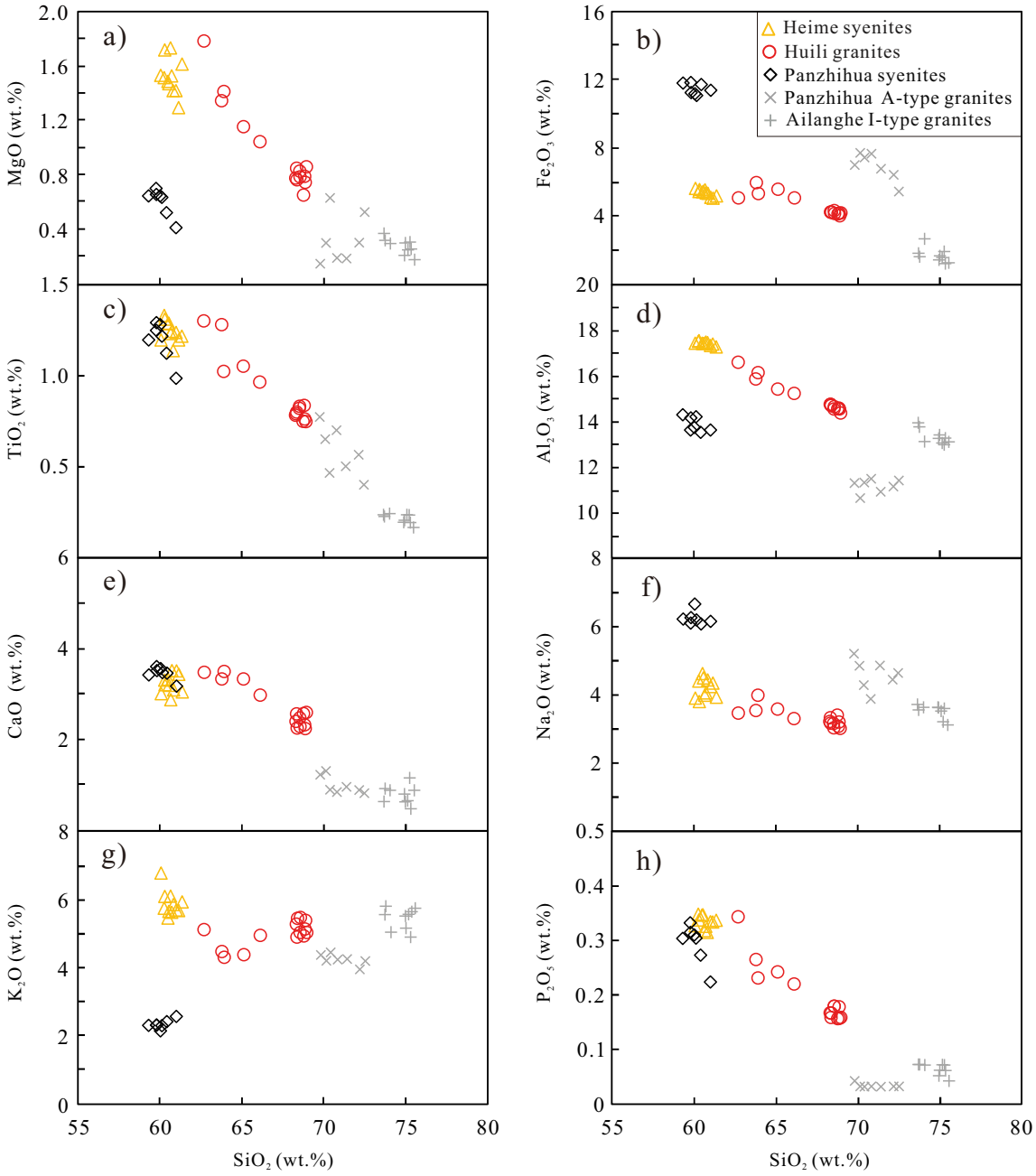

Fig. 8. Plots of major oxide (MgO, Fe_2O_3, TiO_2, Al_2O_3, CaO, Na_2O, K_2O, and P_2O_5) contents vs. SiO_2 for the Heime syenites and Huili granites. All major-element data are recalculated on a volatile-free basis. Considering the affections of alteration, the major-oxide contents of some Heime syenites (CaO < 2.27 wt% and LOI > 4.61 wt%) and Huili granites (CaO < 2.18 wt%) are not presented in these plots. Data for the Panzhihua syenites and A-type granites are from Zhong et al. (2009); data for the Ailanghe I-type granites are from Zhong et al. (2007).

slightly higher than that of the Panzhihua syenites (T_{Zr} = 676 °C–721 °C; recalculation based on data from Zhong et al. (2009) and Boehnke et al. (2013). The zircon saturation temperatures of the Huili granites (T_{Zr} = 808 °C to 877 °C; Table S5) are similar to the A-type Panzhihua granites (T_{Zr} = 805 °C–927 °C; Zhong et al., 2009), but higher than that of the I-type Ailanghe granites (T_{Zr} = 675 °C–754 °C; Zhong et al., 2007).

4.3.2. *Heme and Huili mafic dykes*

Mafic dykes intruding the Heime syenitic intrusion have SiO_2, TiO_2, MgO, Fe_2O_3, CaO, Cr, and Ni contents of 49.7–56.1 wt% (volatile-free), 2.25–4.71 wt%, 3.38–8.53 wt%, 8.65–14.6 wt%, 4.83–10.2 wt%, 26.2–647 ppm, and 20.8–99.4 ppm respectively, with $Mg^{\#}$ (100 × molar $MgO/(MgO + FeO^T)$) = 43.6–55.9 (Table S5). They are characterised by high Nb/Y ratios of 0.90–1.57 and Ti/Y ratios of 664–944 (except for sample HM1704 at 445), similar to those of the Emeishan mafic dykes (Li et al., 2015; Shellnutt et al., 2008) and the spatially associated high-Ti basalts (Ali et al., 2005; Xiao et al., 2004; Xu et al., 2001, 2003). The Heime mafic dykes have high ΣREE contents of 256–367 ppm, with LREE-enriched and HREE-depleted trace element patterns (La_N = 139–274; $(La/Yb)_N$ = 12.8–23.4; Fig. 11e; Boynton, 1984) and insignificant Eu anomalies (Eu/Eu* = 0.91–1.0). In the primitive-mantle-normalized spider diagram (Fig. 11f; Sun and McDonough, 1989), the rocks display "humped" patterns characterised by variable enrichment in all incompatible elements. They exhibit relatively strong Th enrichment and weak to moderate Nb—Ta depletion relative to La (Nb/La = 0.56–0.76) (Fig. 11f).

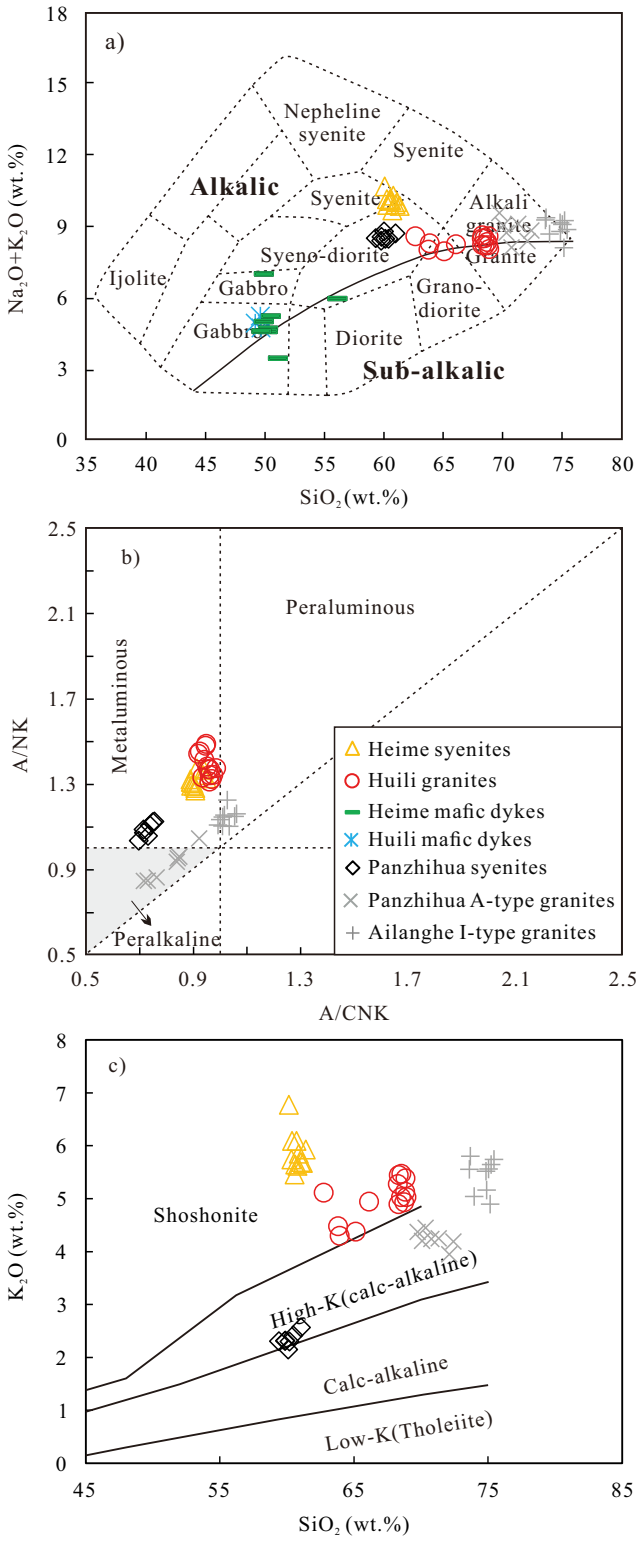

Fig. 9. Plots of (a) ($Na_2O + K_2O$) vs. SiO_2 (Cox et al., 1979); (b) A/NK vs. A/CNK; and (c) K_2O vs. SiO_2 (Peccerillo and Taylor, 1976); for the Heime syenites and Huili granites. Considering the affections of alteration, some Heime syenites (CaO < 2.27 wt% and LOI > 4.61 wt%) and Huili granites (CaO < 2.18 wt %) are not shown in these plots. A/CNK = Al_2O_3/(CaO + Na_2O + K_2O) molar; A/NK = Al_2O_3/(Na_2O+ K_2O) molar. Data sources are as in Fig. 8.

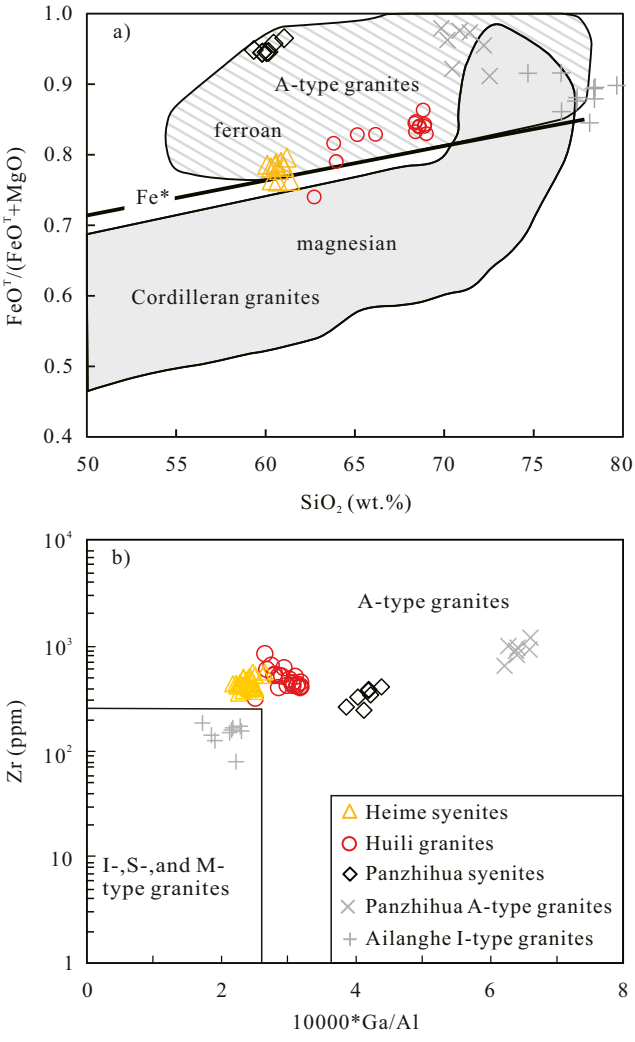

Fig. 10. Plots of (a) $FeO^T/(FeO^T + MgO)$ vs. SiO_2 (Frost et al., 2001) and (b) Zr vs. (10,000 × Ga/Al) (Whalen et al., 1987) for the Heime syenites and Huili granites. Considering the affections of alteration, some Heime syenites (CaO < 2.27 wt% and LOI > 4.61 wt%) and Huili granites (CaO < 2.18 wt%) are not shown in the plots. Data sources are as in Fig. 8.

The mafic dykes intruding the Huili granitic intrusion have SiO_2, TiO_2, MgO, Fe_2O_3, CaO, Cr, and Ni contents of 49.2–50.2 wt%, 3.98–4.27 wt%, 4.56–5.69 wt%, 12.9–14.7 wt%, 7.57–8.59 wt%, 45.1–56.6 ppm, and 66.4–72.2 ppm, respectively, with $Mg^{\#}$ values of 38.0–46.4. The Huili mafic dykes also have high Nb/Y ratios (1.04–1.14) and Ti/Y ratios (664–808), showing an affinity for the Emeishan high-Ti basalts (Ali et al., 2005; Xiao et al., 2004; Xu et al., 2001, 2003). These rocks also show enrichment in LREE and depletion in HREE (La_N = 135–145; $(La/Yb)_N$ = 10.3–13.3; $(La/Sm)_N$ = 2.54–2.68; $(Gd/Yb)_N$ = 2.45–3.47) without significant Eu anomalies (Eu/Eu* = 0.98–1.01). Compared with the Heime mafic dykes, the Huili mafic dykes have relatively low ΣREE contents (231–249 ppm) and less steeply inclined REE patterns (Fig. 11e). In the primitive-mantle-normalized spider diagram (Fig. 11f), they also show "humped" patterns characterised by variable enrichment in all incompatible elements with slightly depleted in Nb and Ta (Nb/La = 0.74–0.95). Thus, all samples from Heime and Huili mafic dykes show ocean-island basalt (OIB) trace- elemental characteristics similar to the Emeishan high-Ti basalts (Fig. 11e and f; Xiao et al., 2004; Xu et al., 2001).

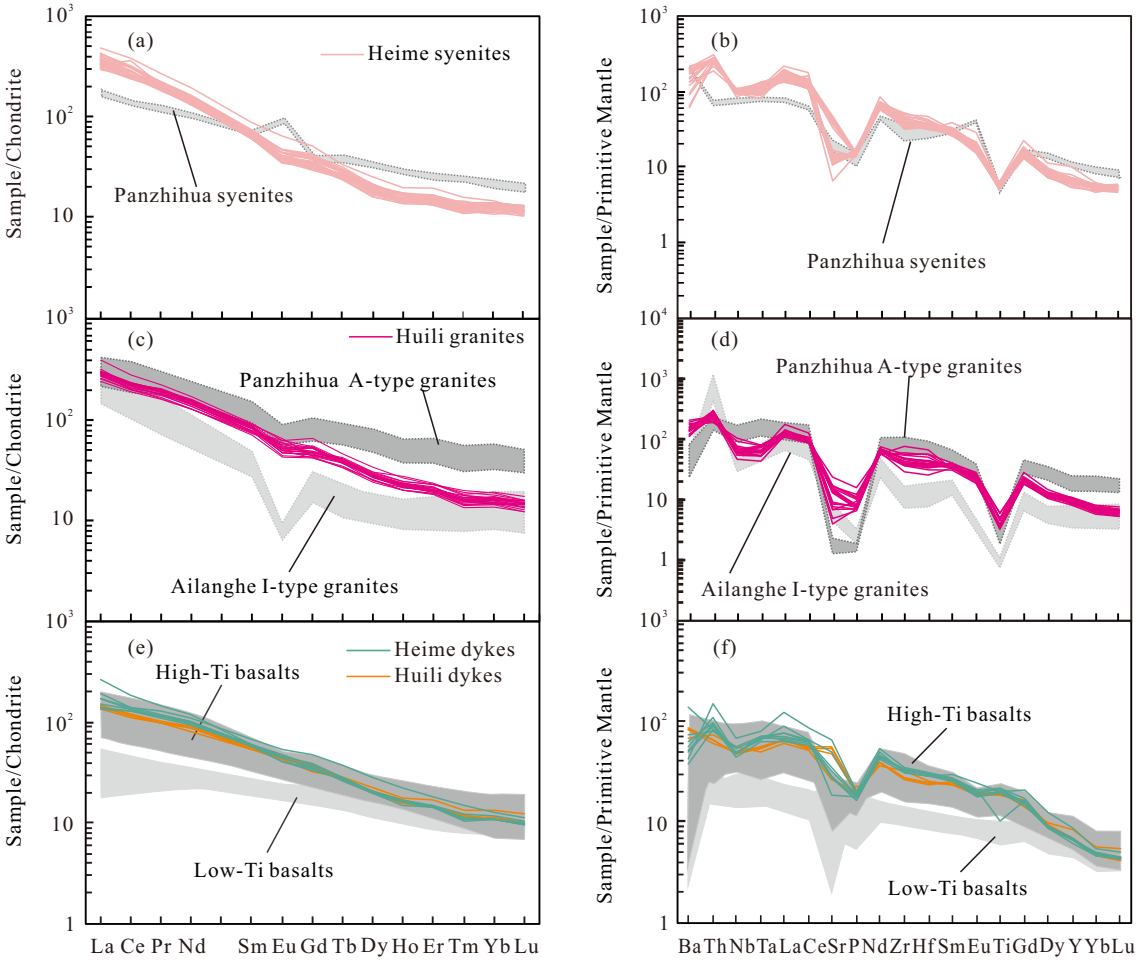

Fig. 11. Chondrite-normalized REE diagrams and primitive-mantle-normalized incompatible trace-element spidergrams for the Heime syenites (a, b), Huili granites (c, d), and mafic dykes (e, f). Chondrite-normalizing values are from Boynton (1984); primitive-mantle-normalizing values are from Sun and McDonough (1989). Data for the Panzhihua syenites and A-type granites are from Zhong et al. (2009); data for the Ailanghe I-type granites are from Zhong et al. (2007); data for the high-Ti and Low-Ti ELIP basalts are from Xiao et al. (2004) and Xu et al. (2001).

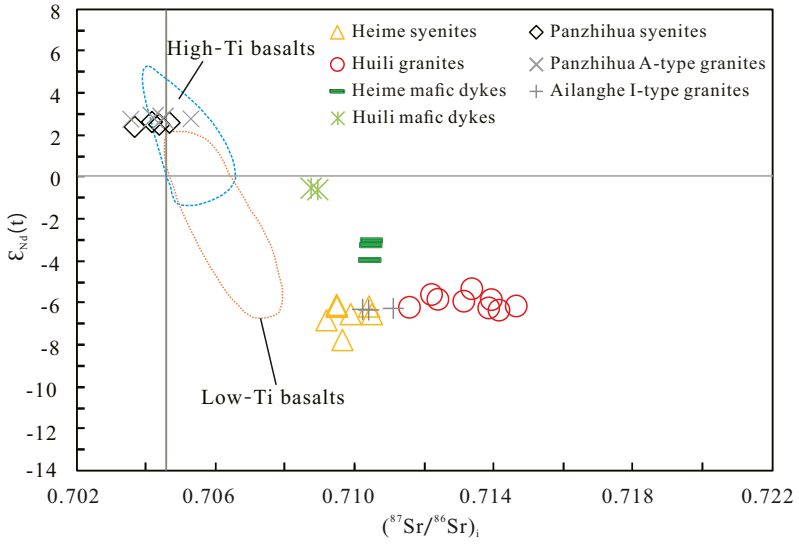

Fig. 12. Plot of whole-rock ε_{Nd} values vs. $(^{87}Sr/^{86}Sr)_i$ ratios for the Heime syenites and Huili granites. Data for high-Ti and low-Ti ELIP basalts are from Ali et al. (2005), Xiao et al. (2004), and Xu et al. (2001, 2003); data for the Panzhihua syenites and A-type granites are from Zhong et al. (2009); data for the Ailanghe I-type granites are from Zhong et al. (2007).

4.4. Whole-rock Sr—Nd isotopic compositions

Whole-rock Sr—Nd isotopic compositions are presented in Table S6 and Fig. 12. The eight analysed samples of Heime syenites have narrow ranges of $^{87}Rb/^{86}Sr$ (0.3796–1.9349) and $^{87}Sr/^{86}Sr$ (0.710867–0.717335) ratios, with initial $(^{87}Sr/^{86}Sr)_i$ values of 0.7092–0.7105 (Table S6). They also have narrow ranges of $^{147}Sm/^{144}Nd$ (0.0782–0.0947) and $^{143}Nd/^{144}Nd$ (0.512064–0.512139) ratios, with $\varepsilon_{Nd}(t)$ values of −7.77 to −6.09, lower than those of the Panzhihua syenites (Table S6; Fig. 12). Two-stage Nd model ages (T^{Nd}_{2DM}) of the Heime syenites are in the range of 1.50–1.37 Ga.

The Huili granites have wider ranges of $^{87}Rb/^{86}Sr$ (1.2435–12.659) and $^{87}Sr/^{86}Sr$ (0.716973–0.758388) ratios, with higher $(^{87}Sr/^{86}Sr)_i$ ratios (0.7116–0.7146) than the Ailanghe I-type and Panzhihua A-type granites (Fig. 12). Their $^{147}Sm/^{144}Nd$ and $^{143}Nd/^{144}Nd$ ratios and $\varepsilon_{Nd}(t)$ values are in the ranges of 0.1059–0.1362, 0.512168–0.512217, and −6.34 to −5.32, respectively, with T^{Nd}_{2DM} ages of 1.38–1.30 Ga (Table S6).

The Heime mafic dykes have $\varepsilon_{Nd}(t)$ values of −3.95 to −3.01 and moderately elevated $(^{87}Sr/^{86}Sr)_i$ ratios of 0.7104–0.7105. The Huili mafic dykes exhibit mostly primitive-mantle-like $\varepsilon_{Nd}(t)$ values from −0.58 to −0.51 and slightly elevated $(^{87}Sr/^{86}Sr)_i$ ratios of 0.7087–0.7089. Thus, the spatially associated Heime and Huili mafic dykes are characterised by significantly higher $\varepsilon_{Nd}(t)$ values than those of the Heime syenites and Huili granites (Table S6; Fig. 12).

5. Discussion

5.1. Alteration effects on major and trace elements

The effects of alteration on major and trace elements of the Heime syenites and Huili granites should be evaluated before using them to discuss their genesis. Zirconium in the igneous rocks is generally considered to be immobile during alteration (e.g., Gibson et al., 1982; Wood et al., 1979). A number of elements were plotted versus Zr contents to evaluate their mobility during alteration (Fig. S1). Apart from Rb, Sr and Ba, other trace elements are tightly correlated with Zr, suggesting that these elements were largely immobile during alteration of the syenites and granites. In addition, according to the relationships between major elements contents (volatile-free) and zirconium (Fig. S2) and LOI values (Fig. S3) of the Heime syenites and Huili granites, it is proposed that CaO, Na_2O, and K_2O contents of some Heime syenites (CaO < 2.27 wt% and LOI > 4.61 wt%) and Huili granites (CaO < 2.18 wt%) were likely mobile during alteration (Figs. S2 and S3). Thus, the major elements of the Heime syenites with CaO < 2.27 wt% and LOI > 4.61 wt% and Huili granites with CaO < 2.18 wt% were excluded from the dataset in following results and discussion. Apart from these samples, the major elements of the other Heime syenites and Huili granites also show good correlations with TiO_2 contents (Fig. S4), implying that the variations of these elements were not controlled by alteration, and therefore can be used for the following petrogenetic discussions.

5.2. Association with the ELIP

Previous SIMS, LA–ICP–MS and CA–TIMS zircon U—Pb dating studies have clearly shown that the voluminous magmatism of the ELIP occurred at ca. 260 Ma (Shellnutt et al., 2012; Zhong et al., 2011). Our new SIMS and LA–ICP–MS dating results for the Heime syenites (259.9 ± 1.9 Ma and 259.8 ± 2.7 Ma) and Huili granites (259.4 ± 1.2 Ma and 260.9 ± 2.8 Ma), and SIMS baddeleyite dating of the Huili mafic dykes (260.8 ± 3.6 Ma) indicate that they were formed contemporaneously at ca. 260 Ma, being a part of the ELIP igneous system.

The spatially associated mafic dykes have high TiO_2 contents (Heime mafic dykes, 2.25–4.71 wt%; Huili mafic dykes, 3.98–4.27 wt%) and Ti/Y (Heime mafic dykes, 445–944; Huili mafic dykes, 664–808) and Nb/Y (Heime mafic dykes, 0.90–1.57; Huili mafic dykes, 1.04–1.14) ratios. Specifically, the Huili dykes have primitive-mantle-like $\varepsilon_{Nd}(t)$ values (−0.58 to −0.51) and display OIB-like trace-element characteristics with insignificant Nb—Ta depletion (Nb/La = 0.74–0.95), similar to high-Ti basalts of the ELIP (Figs. 11e–f and 12; Xiao et al., 2004; Xu et al., 2001). The Heime dykes have relatively low $\varepsilon_{Nd}(t)$ values (−3.95 to −3.01) with slight Nb—Ta depletion (Nb/La = 0.56–0.76), likely due to crustal contamination. Therefore, the studied syenitic and A-type granitic intrusions and mafic dykes within the Pan–Xi area are a part of the ELIP.

5.3. Petrogenesis of the Heime syenites and Huili A-type granites

5.3.1. Petrogenesis of the Heime syenites

Parental magmas of syenites could be generated by different ways (Jahn et al., 2009; Litvinovsky et al., 2015), including (1) fractional crystallisation of K-rich basaltic–andesitic magmas (Brown and Becker, 1986; Shellnutt et al., 2009b, 2011; Thorpe and Tindle, 1992, 2) mixing of mantle-derived basic and crustal-derived silicic magmas followed by differentiation of hybrid monzonitic melts (Sheppard, 1995; Wickham et al., 1995; Zhao et al., 1995), and (3) partial melting of crustal rocks (Litvinovsky et al., 2000; Lubala et al., 1994; Lynch et al., 1993).

The Heime syenites have strongly negative Nb—Ta anomalies, whereas the spatially associated Heime mafic dykes show slightly negative Nb—Ta anomalies (Fig. 11b). Furthermore, the Heime syenites have lower $\varepsilon_{Nd}(t)$ values (−7.77 to −6.09) than those of the Heime high-Ti mafic dykes ($\varepsilon_{Nd}(t)$ = −3.95 to −3.01) (Table S6), indicating that they were not produced by the extreme differentiation of the contemporaneous high-Ti basaltic magma (Fig. 11). It is noteworthy that the zircon $\varepsilon_{Hf}(t)$ values of the syenites exhibit a relatively large variation range from −7.08 to −2.97, which may be resulted from disequilibrium melting of zircon at the source (Tang et al., 2014). However, the relatively constant Nd isotopic compositions and zircon $\delta^{18}O$ values (5.73‰–6.40‰) of the Heime syenites suggest that their parental magmas did not experience significant crustal contamination (Figs. 7a and 12; Table S7). In addition, the Sr–Nd–Hf isotopic compositions of the Heime syenites are clearly different to those of the Panzhihua syenites ($(^{87}Sr/^{86}Sr)_i$ = 0.7041–0.7046; $\varepsilon_{Nd}(t)$ = +2.65, $\varepsilon_{Hf}(t)$ = +6.48 to +9.68; Zhong et al., 2009, 2011). The Sr–Nd–Hf isotopic compositions of the Heime syenites are also different to those of typical mafic–ultramafic intrusions in the inner zone of the ELIP. Previously studied gabbros and pyroxenites from giant mafic–ultramafic layered intrusions generally have positive values of $\varepsilon_{Nd}(t)$ and $\varepsilon_{Hf}(t)$, and relatively low $(^{87}Sr/^{86}Sr)_i$ values (Table S7; Tang et al., 2021; Zhong et al., 2011). Therefore, the geochemical and Sr–Nd–Hf isotopic characteristics of the Heime syenites suggest that they are unrelated to fractional crystallisation of coeval high-Ti basaltic magmas or partial melting of the underplated high-Ti mafic rocks.

The Nd isotopic compositions of the Heime syenites are comparable with those of the contemporaneous Emeishan low-Ti basalts (Fig. 12; Ali et al., 2005; Xiao et al., 2004; Xu et al., 2001, 2003). However, the spatially associated Heime mafic dykes show an affinity for the Emeishan high-Ti basalts rather than low-Ti basalts, providing geological evidence for the development of high-Ti basaltic magma chamber beneath Heime. The Emeishan low-Ti basalts display a lower La/Yb ratios in comparison to the high-Ti basalts (Fig. 11e and f; Ali et al., 2005; Xiao et al., 2004; Xu et al., 2001, 2003). The syenites that are considered to be genetically associated with high-Ti basaltic magma (e.g., the Panzhihua syenites) generally display elevated La/Yb ratios. Moreover, the Heime syenites have higher LREE contents and La/Yb ratios than those of the Panzhihua syenites (Fig. 11a), which is inconsistent with a model that the magmas parental to the Heime syenites were produced by extreme differentiation of the contemporaneous low-Ti basaltic magma.

Although the Sr–Nd–Hf isotopic compositions of the Heime syenites are similar to those of the contemporaneous Ailanghe I-type granites (Table S7; Figs. 7 and 12; Zhong et al., 2007, 2011), zircon $\delta^{18}O$ values of the Heime syenites are similar to those of mantle-derived zircons from

the Panzhihua gabbros (5.49‰–6.10‰), Hongge pyroxenites (5.77‰–6.45‰), and Taihe gabbros (4.12‰–4.56‰) (Table S7; Tang et al., 2021), and significantly lower than those of the Ailanghe I-type granites (7.2‰; unpublished data) (Fig. 7b). It is suggested that the parental magmas of the Heime syenites were different from those of the Ailanghe I-type granites (Fig. 7b), which were likely derived by partial melting of Paleo–Mesoproterozoic meta-sedimentary and meta-volcanic rocks in the western Yangtze Block (Zhong et al., 2007, 2011). The fairly constant zircon $\delta^{18}O$ and whole-rock $\varepsilon_{Nd}(t)$ values also argue against the parental magmas of the Heime syenites were generated by the magma mixing between the mantle-derived basic and crustal-derived silicic magmas (Figs. 7b and 12). Indeed, the whole-rock T^{Nd}_{2MD} ages of 1.50–1.37 Ga and zircon T^{Hf}_{2MD} ages of 1.73–1.42 Ga for the Heime syenite samples (Fig. 7a; Tables S4 and S6) suggest that the magmas parental to the Heime syenites were possibly derived from the partial melting of ancient Yangtze continental crust. Recalculated Nd isotopic compositions of the 1.7 Ga Hekou gabbros of the western Yangtze Block ($\varepsilon_{Nd}(t) = -7.04$ to -3.99 at 260 Ma; Zhu et al., 2017b) are close to those of the Heime syenites. Thus, the mantle-like zircon $\delta^{18}O$ values for the Heime syenites suggest that parental magmas of the Heime syenites were generated by partial melting of Paleo–Mesoproterozoic mafic meta-igneous rocks in the western Yangtze Block (Fig. 7b).

The Heime syenites are characterised by uniform and moderate SiO_2 contents (60.1–61.4 wt%), and high total-alkali ($K_2O + Na_2O$ = 9.68–10.7 wt%) and K_2O (5.46–6.78 wt%) contents, with K_2O/Na_2O ratios of >1 (Figs. 8, 9a and c). Based on these geochemical characteristics, the Heime syenites are classified as K-rich metaluminous syenites (Figs. 9a–c). Furthermore, their relatively constant contents of major oxides in the Heime syenites imply that their parental magmas underwent limited degrees of fractional crystallisation in the deep magma reservoir (Table S5; Fig. 8). In addition, weak negative Eu anomalies indicate negligible plagioclase fractionation during ascent of the parental magma (Fig. 11a). These geochemical characteristics indicate that the magmas parental to the Heime syenites were K-rich metaluminous syenitic magmas.

5.3.2. *Petrogenesis of the Huili A-type granites*

The Huili granites are K-rich metaluminous A-type granites, featured by high total-alkali ($K_2O + Na_2O$ = 7.96–8.62 wt%), and K_2O (4.30–5.47 wt%) contents with K_2O/Na_2O ratios >1 (Figs. 9 and 10). The granites have relatively higher MgO, TiO_2, Al_2O_3, CaO, K_2O, and P_2O_5 contents, and lower SiO_2, $Fe_2O_3^T$, and Na_2O contents than those of the Panzhihua A-type granites (Fig. 8; Zhong et al., 2009). They also have relatively lower REE contents, with more obviously differentiated LREE–HREE patterns and stronger Nb—Ta depletion than the Panzhihua A-type granites (Fig. 10 and Fig. 11; Zhong et al., 2009). Furthermore, the Sr–Nd–Hf isotopic characteristics of the Huili granites are different to those of mantle-derived A-type granites that are temporally and spatially associated with giant layered mafic–ultramafic intrusions in the ELIP (Table S7; Fig. 12; Shellnutt and Zhou, 2007; Shellnutt et al., 2009b; Xu et al., 2008; Zhong et al., 2007, 2009, 2011). These differences in elemental and Sr–Nd–Hf isotopic characteristics between the Huili granites and mantle-derived A-type granites are most likely due to their different magmatic sources.

The Sr—Nd isotopic data of the Huili granites ($(^{87}Sr/^{86}Sr)_i$ = 0.7116–0.7146; $\varepsilon_{Nd}(t) = -6.34$ to -5.32) are obviously different to those of the spatially associated mafic dykes ($\varepsilon_{Nd}(t) = -0.58$ to -0.51) (Fig. 12). Their Sr–Nd–Hf isotopic compositions ($\varepsilon_{Hf}(t) = -3.30$ to +0.73) are also different from those of gabbros and pyroxenites from the mafic–ultramafic layered intrusions (Table S7; Tang et al., 2021; Zhong et al., 2011). Especially, the Huili granites have relatively higher zircon $\delta^{18}O$ values (5.98‰–7.52‰) than those of mantle-derived zircons from the Panzhihua, Hongge, and Taihe mafic–ultramafic rocks (Table S7; Tang et al., 2021). These characteristics suggest that the Huili granites were produced by neither fractionation of contemporaneous basaltic magma, nor partial melting of juvenile mafic crust.

The Huili granites share similar Sr—Nd isotopic (Fig. 12) and trace elemental characteristics with strong negative Nb—Ta anomalies with the Heime syenites (Figs.11a–11d). However, the Huili granites have higher $\delta^{18}O$ (5.98‰–7.52‰) and $\varepsilon_{Hf}(t)$ (-3.3 to +0.73) values than those of the Heime syenites ($\delta^{18}O$ = 5. 73‰–6.40‰; $\varepsilon_{Hf}(t) = -7.08$ to -2.97; Table S4; Fig. 7). This also suggests that the parental magmas of the Huili granites and the Heime syenites were derived from different magmatic sources.

The Sr—Nd isotopic compositions of the Huili granites are similar to those of the Ailanghe I-type granites ($\varepsilon_{Nd}(t) = -7.44$ to -6.30; $(^{87}Sr/^{86}Sr)_i$ = 0.7102–0.7111) (Table S7; Fig. 12; Zhong et al., 2007, 2011). The whole-rock T^{Nd}_{2MD} ages of 1.38–1.30 Ga and zircon T^{Hf}_{2MD} ages of 1.49–1.23 Ga of the Huili granites also close to those of the Ailanghe I-type granites (Zhong et al., 2007, 2011), implying that the parental magmas of the Huili granites were mainly derived from partial melting of Paleo–Mesoproterozoic meta-sedimentary and meta-volcanic rocks in the western Yangtze Block. However, the Huili granites have relatively high $\varepsilon_{Hf}(t)$ (-3.30 to +0.73) and low zircon $\delta^{18}O$ values (5.98–7.52‰) compared with the Ailanghe I-type granites ($\varepsilon_{Hf}(t) = -0.89$ to -6.33; $\delta^{18}O$ = 7.2‰; Fig. 7; Zhong et al., 2011; unpublished data). In the zircon $\delta^{18}O$–$\varepsilon_{Hf}(t)$ diagram (Fig. 7b; Kemp et al., 2007), $\delta^{18}O$ and $\varepsilon_{Hf}(t)$ values of the Huili granites are negatively correlated, and plot between those of Ailanghe granites and Huili mafic dykes. The maximum zircon $\delta^{18}O$ value of the Huili granites is similar to that of the Ailanghe I-type granites, and both their minimum zircon $\delta^{18}O$ and maximum $\varepsilon_{Hf}(t)$ values of the Huili granites are similar to those of mantle-derived basaltic magmas (Fig. 7b). Based on the linear relationship between $\delta^{18}O$ and $\varepsilon_{Hf}(t)$ values (Fig. 7b; Kemp et al., 2007), the parental magma of the Huili granites may have been a mixture of two magmas, with the main magma having high $\delta^{18}O$ and negative $\varepsilon_{Hf}(t)$ values derived from partial melting of ancient basement rocks, and the subordinate magma having low $\delta^{18}O$ and positive $\varepsilon_{Hf}(t)$ values from coeval mantle-derived basaltic magma.

The granites have moderate to high SiO_2 contents (62.7–68.9 wt%) and display systematic change in chemical composition from alkaline syenodioritic to granitic rocks (Table S5; Figs. 8 and 9a). Moreover, the granites have relatively wide ranges of SiO_2, MgO, Fe_2O_3, TiO_2, Al_2O_3, and P_2O_5 contents (Table S5; Fig. 8), indicating fractional crystallisation of Mg–Fe–Ti–Al–P-rich minerals in the deep magma reservoir. Their MgO and Fe_2O_3 contents decrease with increasing SiO_2 content (Table S5; Fig. 8) may result from fractionation of Mg- and Fe-rich minerals (e.g., hornblende and augite). The decrease in P_2O_5 content with increasing SiO_2 content suggests the fractionation of apatite (Fig. 9). The slightly negative correlation of Na_2O versus SiO_2 and positive correlation of K_2O versus SiO_2 may reflect small degree of plagioclase fractionation and K-feldspar crystallisation in the deep magma reservoir (Fig. 8). The negative correlation of Zr with SiO_2 indicates the fractionation of zircon (Fig. S2), consistent with zircon saturation in the evolving melt. As discussed above, the systematic variation in chemical compositions from syenodioritic to granitic rocks suggests that the Huili A-type granites were likely formed by fractional crystallisation of syenitic magma in the deep magma reservoir (Litvinovsky et al., 2002). Thus, the magmas parental to the Huili granites also exhibit the K-rich metaluminous syenitic magmas.

5.4. *Genesis of syenites and A-type granites within the ELIP*

Our new zircon and baddeleyite U—Pb dating results suggest that the Heime syenites, Huili granites, and spatially associated mafic dykes were formed at ca. 260 Ma, in association with the eruption and emplacement of Emeishan mafic magmas. Based on our new geochemical and Sr–Nd–O–Hf isotopic data of the Heime syenites and A-type Huili granites, we suggest that the K-rich syenitic magmas parental to the two intrusions were mainly generated by partial melting of Paleo– to Mesoproterozoic crust. The Paleo- to Mesoproterozoic Tong'an–Huili groups and its equivalents, comprising low-grade meta-sedimentary

rocks and meta-volcanic rocks with mafic intrusions, occur widely in the Pan–Xi area (Fan et al., 2020). The parental magmas of the Heime syenites were likely derived from partial melting of Paleo–Mesoproterozoic mafic meta-igneous rocks in the western Yangtze Block, whereas those of the A-type Huili granites were generated by partial melting of Paleo–Mesoproterozoic basement rocks with a portion of coeval mantle-derived basaltic magma.

The calculated zircon saturation temperatures (T_{Zr}) for the Heme syenites and Huili granites are 764 °C –814 °C and 808 °C–877 °C, respectively (Table S5). Especially, the T_{Zr} of the Huili granites are very similar to those of the Panzhihua A-type granites (805 °C–927 °C; Zhong et al., 2009), but obviously higher than those of the Ailanghe I-type granites (675 °C–754 °C; Zhong et al., 2007). It is suggested that the parental magmas of the Huili granites were formed at relatively high temperatures. The large heat for the melting of the source of the Huili granites likely came from Emeishan magmatic reservoir as evidenced by the tempospatially-associated mafic dykes. Regarding that the maximum temperature of mantle-derived basaltic magmas in the ELIP might have exceeded 1500 °C (Xu et al., 2001; Yao et al., 2021), the upwelling of hot voluminous mantle-derived basaltic magma in the ELIP can serve as an important heat source for partial melting of ancient crustal rocks. In other words, heat from the underplating and/or intrusion of anomalously hot basaltic magmas of the Emeishan mantle plume could lead to partial melting of the most fusible portions from the overlying Paleo- to Mesoproterozoic crust.

Previous studies have suggested that only some I-type granites (i.e., the Ailanghe and Yingpanliangzi plutons) associated with the ELIP were derived from partial melting of ancient continental crust (Shellnutt et al., 2011; Zhong et al., 2007, 2011; Zhu et al., 2017a). However, our new data suggest that some of the syenites and A-type granites within the inner zone of the ELIP can also be generated by the melting of ancient continental crust rather than by fractional crystallisation of Emeishan mafic magmas or partial melting of underplated mafic rocks during Emeishan magmatism (Shellnutt et al., 2009a, 2009b, 2011; Shellnutt and Jahn, 2010; Shellnutt and Zhou, 2007; Xu et al., 2008; Zhong et al., 2007, 2009, 2011). The recognition of ancient crustal-derived syenites and A-type granites, together with results of previous studies, provides new insights into the petrogenesis of syenites and A-type granites in the ELIP. They could have been formed in at least three different ways, including (1) fractionation of plume-related basaltic magmas (e.g., Taihe, Baima, and Panzhihua A-type granites/syenites; Shellnutt and Jahn, 2010; Shellnutt and Zhou, 2008; Shellnutt et al., 2009b, 2011; Zhong et al., 2007, 2009, 2011); (2) partial melting of juvenile crust (underplated mafic rocks) during Emeishan magmatism (e.g., Huangcao and Woshui syenites; Shellnutt and Jahn, 2010; Shellnutt and Zhou, 2007, 2008; Shellnutt et al., 2009a); and (3) partial melting of ancient continental crust (e.g., Heime syenites and Huili granites). Therefore, the Emeishan mantle plume activity not only gave rise to late Permian large mafic magmatism and significant growth of juvenile crust in the center of the ELIP, but also produced reworking of ancient crust because of the high thermal gradient in crustal level caused by the anomalously plume event.

6. Conclusions

The following conclusions are drawn from this study.

(1) Zircon and baddeleyite U—Pb ages indicate that the Heime syenites, Huili granites, and spatially associated mafic dykes were intruded at ca. 260 Ma, corresponding to the eruption and emplacement of mafic magmatism of the ELIP.
(2) The Heime syenites are typical K-rich syenites and the Huili granites exhibit features of K-rich A-type granites. They display relatively low $\varepsilon_{Nd}(t)$ values (Heime syenites, −7.77 to −6.09; Huili granites, −6.34 to −5.32) and high $(^{87}Sr/^{86}Sr)_i$ ratios (Heime syenites, 0.7092–0.7105; Huili granites, 0.7116–0.7146). Zircons of the Heime syenites have a wide range of negative $\varepsilon_{Hf}(t)$ (−7.08 to −2.97) and are close to the mantle $\delta^{18}O$ values (5.73–6.40‰), indicating that their parental magmas were produced by partial melting of Paleo–Mesoproterozoic mafic meta-igneous rocks. Zircons from the Huili granites have more depleted Hf isotopic compositions ($\varepsilon_{Hf}(t) = -3.30$ to+0.73) and elevated $\delta^{18}O$ values (5.98–7.52‰), suggesting that their parental magmas were derived from partial melting of Paleo–Mesoproterozoic basement rocks and mixing with small amounts of coeval mantle-derived basaltic magma.
(3) The parental magmas of the Heime syenites and Huili A-type granites both exhibit the K-rich metaluminous syenitic magmas. We suggest that the K-rich metaluminous syenitic magmas were derived mainly from partial melting of Paleo–Mesoproterozoic crust, in association with the reworking of ancient crust response to the Emeishan mantle plume.

Supplementary data to this article can be found online at https://doi.org/10.1016/j.lithos.2022.106844.

Declaration of Competing Interest

The authors declare that they have no known competing financial interests or personal relationships that could have appeared to influence the work reported in this paper.

Acknowledgements

This study was financially supported by the National Natural Science Foundation of China (Grants 42121003 and 42172092). We are grateful that Dr. Chusi Li of Indiana University for his constructive suggestions. We also thank Q.L. Li, Y. Liu and G.Q. Tang for their assistance in SIMS zircon dating and O isotope analysis, Y.W. Tang for his assistance in LA–ICP–MS zircon dating, Z.C. Hu and Y.S. Liu for their assistance in LA–ICP–MS zircon Hf isotope analysis, B. Wang for whole-rock major element analyses by XRF, J. Hu, Y. Huang and G.P. Bao for whole-rock trace element analyses by ICP–MS, F. Xiao and J. Wang for whole-rock Sr—Nd isotopes analyses. The paper benefited from review comments from the editor and two anonymous reviewers.

References

Ali, J.R., Thompson, G.M., Zhou, M.F., Song, X.Y., 2005. Emeishan large igneous province, SW China. Lithos 79, 475–489.
Boehnke, P., Watson, E.B., Trail, D., Harrison, T.M., Schmitt, A.K., 2013. Zircon saturation re-revisited. Chem. Geol. 351, 324–334.
Boynton, W.V., 1984. Geochemistry of the rare earth elements: Meteorite studies. In: Henderson, P. (Ed.), Rare Earth Element Geochemistry. Elservier, pp. 63–114.
Brown, P.E., Becker, S.M., 1986. Fractionation, hybridization and magma mixing in the Kialineq center East Greenland. Contrib. Mineral. Petrol. 92, 57–70.
Chen, W.T., Zhou, M.F., Zhao, X.F., 2013. Late Paleoproterozoic sedimentary and mafic rocks in the Hekou area, SW China: Implication for the reconstruction of the Yangtze Block in Columbia. Precambrian Res. 231, 61–77.
Chung, S.L., Jahn, B.M., 1995. Plume-lithosphere interaction in generation of the Emeishan flood basalts at he Perrmain–Triassic boundary. Geology 23, 889–892.
Chung, S.L., Jahn, B.M., Genyao, W., Lo, C.H., Bolin, C., 1998. The Emeishan flood Basalt in SW China: A mantle plume initiation model and its connection with continental breakup and mass extinction at the Permian–Triassic boundary. In: Flower, M.F.J., Chung, S.L., Lo, C.H., Lee, T.Y. (Eds.), Mantle Dynamics and Plate Interactions in East Asia, pp. 47–58.
Cox, K.G., Bell, J.D., Pankhurst, R.J., 1979. In: The Interpretation of Igneous Rocks. Allen and Unwin, London, UK, p. 450.
Fan, H.P., Zhu, W.G., Li, Z.X., 2020. Paleo- to Mesoproterozoic magmatic and tectonic evolution of the southwestern Yangtze Block, south China: New constraints from ca. 1.7–1.5 Ga mafic rocks in the Huili–Dongchuan area. Gondwana Res. 87, 248–262.
Frost, B.R., Barnes, C.G., Collins, W.J., Arculus, R.J., Ellis, D.J., Frost, C.D., 2001. A geochemical classification for granitic rocks. J. Petrol. 42, 2033–2048.
Gibson, S.A., Kirkpatrick, R.J., Emmerman, R., Schmincke, P.H., Pritchard, G., Okay, P. J., Horpe, R.S., Marriner, G.F., 1982. The trace element composition of the lavas and dykes from a 3 km vertical section through a lava pile of Eastern Iceland. J. Geophys. Res. 87, 6532–6546.

Greentree, M.R., Li, Z.X., 2008. The oldest known rocks in south-western China: SHRIMP U–Pb magmatic crystallisation age and detrital provenance analysis of the Paleoproterozoic Dahongshan Group. J. Asian Earth Sci. 33, 289–302.
Griffin, W.L., Wang, X., Jackson, S.E., Pearson, N.J., O'Reilly, S.Y., Xu, X.S., Zhou, X.M., 2002. Zircon chemistry and magma mixing, SE China: In-situ analysis of Hf isotopes, Tonglu and Pingtan igneous complexes. Lithos 61, 237–269.
Guo, C.L., Wang, D.H., Chen, Y.L., Zhao, Z.G., Wang, Y.B., Fu, X.F., Fu, D.M., 2007. SHRIMP U-Pb zircon ages and major element, trace element and Nd-Sr isotope geochemical studies of a Neoproterozoic granitic complex in western Sichuan: Petrogenesis and tectonic significance. Acta Petrol. Sin. 23, 2457–2470.
He, B., Xu, Y.G., Chung, S.L., Xiao, L., Wang, Y., 2003. Sedimentary evidence for a rapid, kilometer-scale crustal doming prior to the eruption of the Emeishan flood basalts. Earth Planet. Sci. Lett. 213, 391–405.
He, D.F., Zhu, W.G., Zhong, H., Ren, T., Bai, Z.J., Fan, H.P., 2013. Zircon U–Pb geochronology and elemental and Sr–Nd–Hf isotopic geochemistry of the Daocheng granitic pluton from the Yidun Arc, SW China. J. Asian Earth Sci. 67–68, 1–17.
Hu, Z.C., Liu, Y.S., Gao, S., Liu, W.G., Zhang, W., Xirun, T., Lin, L., Zong, K.Q., Li, M., Chen, H.H., Zhou, L., Yang, L., 2012. Improved in situ Hf isotope ratio analysis of zircon using newly designed X skimmer cone and jet sample cone in combination with the addition of nitrogen by laser ablation multiple collector ICP–MS. J. Anal. At. Spectrom. 27, 1391–1399.
Jahn, B.M., Litvinovsky, B.A., Zanvilevich, A.N., Reichow, M., 2009. Peralkaline granitoid magmatism in the Mongolian–Transbaikalian Belt: Evolution, petrogenesis and tectonic significance. Lithos 113, 521–539.
Jeon, H., Williams, I.S., Bennett, V.C., 2014. Uncoupled O and Hf isotopic systems in zircon from the contrasting granite suites of the New England Orogen, eastern Australia: Implications for studies of Phanerozoic magma genesis. Geochim. Cosmochim. Acta 146, 132–149.
Kemp, A.I.S., Hawkesworth, C.J., Foster, G.L., Paterson, B.A., Woodhead, J.D., Hergt, J. M., Gray, C.M., Whitehouse, M.J., 2007. Magmatic and crustal differentiation history of granitic rocks from Hf–O isotopes in zircon. Science 315, 980–983.
Li, H., Zhang, Z., Ernst, R., Lü, L., Santosh, M., Zhang, D., Cheng, Z., 2015. Giant radiating mafic dyke swarm of the Emeishan large igneous province: identifying the mantle plume Centre. Terra Nova 27, 247–257.
Li, X.H., Li, Z.X., Zhou, H.W., Ying, L., Liang, X.R., Li, W.X., 2003b. SHRIMP U–Pb zircon age, geochemistry and Nd isotope of the Guandaoshan pluton in SW Sichuan: Petrogenesis and tectonic significance. Sci. China Ser. D 46 (Suppl), 73–83.
Li, X.H., Liu, Y., Li, Q., Guo, C.H., Chamberlain, K.R., 2009. Precise determination of Phanerozoic zircon Pb/Pb age by multicollector SIMS without external standardization. Geochem. Geophys. Geosyst. 10, Q04010 doi:04010.01029/.
Li, X.H., Tang, G.Q., Gong, B., Yang, Y.H., Hou, K.J., Hu, Z.C., Li, Q.L., Liu, Y., Li, W.X., 2013. Qinghu zircon: a working reference for microbeam analysis of U-Pb age and Hf and O isotopes. Chin. Sci. Bull. 58, 4647–4654.
Li, Z.X., Li, X.H., Kinny, P.D., Wang, J., Zhang, S., Zhou, H., 2003a. Geochronology of Neoproterozoic syn-rift magmatism in the Yangtze Craton, South China and correlations with other continents: evidence for a mantle superplume that broke up Rodinia. Precambrian Res. 122, 85–109.
Litvinovsky, B.A., Steel, I.M., Wickham, S.M., 2000. Silicic magma formation in overthickened crust: Melting of charnockite and leucogranite at 15, 20 and 25 kbar. J. Petrol. 41, 717–737.
Litvinovsky, B.A., Jahn, B.M., Zanvilevich, A.N., Saunders, A., Poulain, S., Kuzmin, D.V., Reichow, M.K., Titov, A.V., 2002. Petrogenesis of syenite–granite suites from the Bryansky complex (Transbaikalia, Russia): implications for the origin of A-type granitoid magmas. Chem. Geol. 189, 105–133.
Litvinovsky, B.A., Jahn, B.M., Eyal, M., 2015. Mantle-derived sources of syenites from the A-type igneous suites —New approach to the provenance of alkaline silicic magmas. Lithos 232, 242–265.
Lubala, R.T., Frick, C., Roders, J.H., Walraven, F., 1994. Petrogenesis of syenites and granites of the Schiel Alkaline complex, Northern Transvaal, Southern Africa. J. Geol. 102, 307–309.
Lynch, D.J., Musselman, T.E., Gutmann, J.T., Patchett, P.J., 1993. Isotopic evidence for the origin of Cenozoic volcanic rocks in the Pinacate volcanic field, northwestern Mexico. Lithos 29, 295–302.
Peccerillo, A., Taylor, S., 1976. Geochemistry of Eocene Calc-alkaline volcanic rocks from the Kastamonu Area, Northern Turkey. Contrib. Mineral. Petrol. 58, 63–81.
Qi, L., Hu, J., Conrad, D., 2000. Determination of trace elements in granites by inductively coupled plasma mass spectrometry. Talanta 51, 507–513.
SBG (Sichuan Bureau of Geology), 1966. A Report of Regional Geological Survey in Miyi Area of the People's Republic of China (the scale of 1:200000) (in Chinese).
SBG (Sichuan Bureau of Geology), 1978. A Report of Regional Geological Survey in Sichuan Province of the People's Republic of China (the scale of 1:500000) (in Chinese).
Shellnutt, J.G., 2014. The Emeishan large igneous province: a synthesis. Geosci. Front. 5, 369–394.
Shellnutt, J.G., 2021. A cumulate syenite in the upper part of the Hongge layered mafic intrusion, Emeishan large igneous province, SW China. Int. J. Earth Sci. 110, 2979–3000.
Shellnutt, J.G., Jahn, B.M., 2010. Formation of the late Permian Panzhihua plutonic-hypabyssal-volcanic igneous complex: Implications for the genesis of Fe–Ti oxide deposits and A-type granites of SW China. Earth Planet. Sci. Lett. 289, 509–519.
Shellnutt, J.G., Zhou, M.F., 2007. Permian peralkaline, peraluminous and metaluminous A-type granites in the Panxi district, SW China: their relationship to the Emeishan mantle plume. Chem. Geol. 243, 286–316.
Shellnutt, J.G., Zhou, M.F., 2008. Permian, rifting related fayalite syenite in the Panxi region, SW China. Lithos 101, 54–73.
Shellnutt, J.G., Zhou, M.F., Yan, D.P., Wang, Y., 2008. Longevity of the Permian Emeishan mantle plume (SW China): 1 million years; 8 million years or 18 million years? Geol. Mag. 145, 373–388.
Shellnutt, J.G., Wang, C.Y., Zhou, M.F., Yang, Y.H., 2009a. Zircon Lu–Hf isotopic compositions of metaluminous and peralkaline A-type granitic plutons of the Emeishan large igneous province (SW China): constraints on the mantle source. J. Asian Earth Sci. 35, 45–55.
Shellnutt, J.G., Zhou, M.F., Zellmer, G.F., 2009b. The role of Fe–Ti oxide crystallization in the formation of A-type granitoids with implications for the Daly gap: an example from the Permian Baima igneous complex, SW China. Chem. Geol. 259, 204–217.
Shellnutt, J.G., Jahn, B.M., Zhou, M.F., 2011. Crustal-derived granites in the Panzhihua region, SW China: implications for felsic magmatism in the Emeishan large Igneous province. Lithos 123, 145–157.
Shellnutt, J.G., Denyszyn, S.W., Mundil, R., 2012. Precise age determination of mafic and felsic intrusive rocks from the Permian Emeishan large igneous province (SW China). Gondwana Res. 22, 118–126.
Shellnutt, J.G., Pham, T.T., Denyszyn, S.W., Yeh, M.-W., Tran, T.A., 2020. Magmatic duration of the Emeishan large igneous province: insight from Northern Vietnam. Geology 48, 457–461.
Sheppard, S., 1995. Hybridization of shoshonitic lamprophyre and calc-alkaline granite magma in the early Proterozoic Mt. Bandey igneous suite, Northern Territory. Aus. J. Earth Sci. 42, 173–185.
Sun, S.S., McDonough, W.F., 1989. Chemical and isotopic systematics of oceanic basalts: implications for mantle composition and processes. Geo.Soc.London Spec. Pub. 42, 313–345.
Tang, M., Wang, X.L., Shu, X.J., Wang, D., Yang, T., Gopon, P., 2014. Hafnium isotopic heterogeneity in zircons from granitic rocks: Geochemical evaluation and modeling of "zircon effect" in crustal anatexis. Earth Planet. Sci. Lett. 389, 188–199.
Tang, Q.Y., Li, C.S., Ripley, E.M., Bao, J., Su, T.B., Xu, S.H., 2021. Sr–Nd–Hf–O isotope constraints on crustal contamination and mantle source variation of three Fe–Ti–V oxide ore deposits in the Emeishan large igneous province. Geochim. Cosmochim. Acta 292, 364–381.
Thorpe, R.S., Tindle, A.G., 1992. Petrology and Petrogenesis of a Tertiary bimodal dolerite-peralkaline/ subalkaline trachytehhyolite dyke association from Lundy, Bristol Channel, UK. Geol. J. 27, 101–117.
Valley, J.W., 2003. Oxygen isotopes in zircon. In: Hanchar, J.M., Hoskin, P.W.O. (Eds.), Zircon, pp. 343–385.
Valley, J.W., Kinny, P.D., Schulze, D.J., Spicuzza, M.J., 1998. Zircon megacrysts from kimberlite: oxygen isotope variability among mantle melts. Contrib. Mineral. Petrol. 133, 1–11.
Vervoort, J.D., Patchett, P.J., Blichert-Toft, J., Albarede, F., 1999. Relationships between Lu-Hf and Sm-Nd isotopic systems in the global sedimentary system. Earth Planet. Sci. Lett. 168, 79–99.
Whalen, J.B., Currie, K.L., Chappell, B.W., 1987. A-type granites: geochemical characteristics, discrimination and petrogenesis. Contrib. Mineral. Petrol. 95, 407–419.
Wickham, S.M., Litvinovsky, B.A., Zanvilevich, A.N., Bindeman, I.N., Schauble, E.A., 1995. Geochemical evolution of Phanerozoic magmatism in Transbaikalia, East Asia: a key constraint on the origin of K-rich silicic magmas and the process of cratonization. J. Geophys. Res. 100, 15641–15654.
Wood, D.A., Joron, J.L., Treuil, M., 1979. A re-appraisal of the use of trace elements to classify and discriminate between magma series erupted in different tectonic settings. Earth Planet. Sci. Lett. 45, 326–336.
Xiao, L., Xu, Y.G., Mei, H.J., Zheng, Y.F., He, B., Pirajno, F., 2004. Distinct mantle sources of low-Ti and high-Ti basalts from the western Emeishan large igneous province, SW China: implications for plume–lithosphere interaction. Earth Planet. Sci. Lett. 228, 525–546.
Xu, Y.G., Chung, S.L., Jahn, B.M., Wu, G.Y., 2001. Petrologic and geochemical constraints on the petrogenesis of Permian–Triassic Emeishan flood basalts in southwestern China. Lithos 58, 145–168.
Xu, Y.G., Mei, H.J., Xu, J.G., Huang, X.L., Wang, Y.J., Chung, S.L., 2003. Origin of two differentiation trends in the Emeishan flood basalts. Chin. Sci. Bull. 48, 390–394.
Xu, Y.G., He, B., Chung, S.L., Menzies, M.A., Frey, F.A., 2004. Geologic, geochemical, and geophysical consequences of plume involvement in the Emeishan flood-basalt province. Geology 32, 917–920.
Xu, Y.G., Luo, Z.Y., Huang, X.L., He, B., Xiao, L., Xie, L.W., Shi, Y.R., 2008. Zircon U–Pb and Hf isotope constraints on crustal melting associated with the Emeishan mantle plume. Geochim. Cosmochim. Acta 72, 3084–3104.
Yao, J.H., Zhu, W.G., Wang, Y.J., Zhong, H., Bai, Z.J., 2021. Geochemistry of the Yumen picrites-basalts from the Emeishan large igneous province: Implications for their mantle source, PGE behaviors, and petrogenesis. Lithos 400–401, 106364.
YBG (Yunnan Bureau of Geology), 1966. A Report of Regional Geological Survey in Yongren Area of the People's Republic of China (the scale of 1:200000) (in Chinese).
Zhang, Z.Z., Qin, J.F., Lai, S.C., Long, X.P., Ju, Y.J., Wang, X.Y., Zhu, Y., Zhang, F.Y., 2021. High-temperature melting of different crustal levels in the inner zone of the Emeishan large igneous province: Constraints from the Permian ferrosyenite and granite from the Panxi region. Lithos 402–403, 105979.
Zhao, J.X., Shiraishi, K., Ellis, D.J., Sheratin, J.W., 1995. Geochemical and isotopic studies of syenites from the Yamato Mountains, East Antarctica: Implications of the origin of syenitic magmas. Geochim. Cosmochim. Acta 59, 1363–1382.
Zhao, X.F., Zhou, M.F., Li, J.W., Sun, M., Gao, J.F., Sun, W.H., Yang, J.H., 2010. Late Paleoproterozoic to early Mesoproterozoic Dongchuan Group in Yunnan, SW China: Implications for tectonic evolution of the Yangtze Block. Precambrian Res. 182, 57–69.

Zhong, H., Zhu, W.G., Chu, Z.Y., He, D.F., Song, X.Y., 2007. Shrimp U–Pb zircon geochronology, geochemistry, and Nd–Sr isotopic study of contrasting granites in the Emeishan large igneous province, SW China. Chem. Geol. 236, 112–133.

Zhong, H., Zhu, W.G., Hu, R.Z., Xie, L.W., He, D.F., Liu, F., Chu, Z.Y., 2009. Zircon U–Pb age and Sr–Nd–Hf isotope geochemistry of the Panzhihua A-type syenitic intrusion in the Emeishan large igneous province, southwest China and implications for growth of juvenile crust. Lithos 110, 109–128.

Zhong, H., Campbell, I.H., Zhu, W.G., Allen, C.M., Hu, R.Z., Xie, L.W., He, D.F., 2011. Timing and source constraints on the relationship between mafic and felsic intrusions in the Emeishan large igneous province. Geochim. Cosmochim. Acta 75, 1374–1395.

Zhou, M.F., Malpas, J., Song, X.Y., Robinson, P.T., Sun, M., Kennedy, A.K., Lesher, C.M., Keays, R.R., 2002a. A temporal link between the Emeishan large igneous province (SW China) and the end-Guadalupian mass extinction. Earth Planet. Sci. Lett. 196, 113–122.

Zhou, M.F., Yan, D.P., Kennedy, A.K., Li, Y.Q., Ding, J., 2002b. SHRIMP U–Pb zircon geochronological and geochemical evidence for Neoproterozoic arc-magmatism along the western margin of the Yangtze Block, South China. Earth Planet. Sci. Lett. 196, 51–67.

Zhou, M.F., Ma, Y.X., Yan, D.P., Xia, X.P., Zhao, J.H., Sun, M., 2006a. The Yanbian Terrane (Southern Sichuan Province, SW China): a Neoproterozoic arc assemblage in the western margin of the Yangtze Block. Precambrian Res. 144, 19–38.

Zhou, M.F., Yan, D.P., Wang, C.L., Qi, L., Kennedy, A., 2006b. Subduction-related origin of the 750 Ma Xuelongbao adakitic complex (Sichuan Province, China): implications for the tectonic setting of the giant Neoproterozoic magmatic event in South China. Earth Planet. Sci. Lett. 248, 286–300.

Zhou, M.F., Arndt, N.T., Malpas, J., Wang, C.Y., Kennedy, A.K., 2008. Two magma series and associated ore deposit types in the Permian Emeishan large igneous province, SW China. Lithos 103, 352–368.

Zhu, B., Peate, D.W., Guo, Z.J., Liu, R.C., Du, W., 2017a. Crustally derived granites in Dali, SW China: new constraints on silicic magmatism of the Central Emeishan large Igneous Province. Int. J. Earth Sci. 106, 2503–2525.

Zhu, W.G., Zhong, H., Deng, H.L., Wilson, A.H., Liu, B.G., Li, C.Y., Qin, Y., 2006. SHRIMP zircon U–Pb age, geochemistry, and Nd–Sr isotopes of the Gaojiacun mafic–ultramafic intrusive complex, Southwest China. Int. Geol. Rev. 48, 650–668.

Zhu, W.G., Zhong, H., Li, X.H., Liu, B.G., Deng, H.L., Qin, Y., 2007. ^{40}Ar–^{39}Ar age, geochemistry and Sr–Nd–Pb isotopes of the Neoproterozoic Lengshuiqing Cu–Ni sulfide-bearing mafic–ultramafic complex, SW China. Precambrian Res. 155, 98–124.

Zhu, W.G., Zhong, H., Li, X.H., Deng, H.L., He, D.F., Wu, K.W., Bai, Z.J., 2008. SHRIMP zircon U–Pb geochronology, elemental, and Nd isotopic geochemistry of the Neoproterozoic mafic dykes in the Yanbian area, SW China. Precambrian Res. 164, 66–85.

Zhu, W.G., Zhong, H., Li, Z.X., Bai, Z.J., Yang, Y.J., 2016. SIMS zircon U–Pb ages, geochemistry and Nd–Hf isotopes of ca. 1.0Ga mafic dykes and volcanic rocks in the Huili area, SW China: Origin and tectonic significance. Precambrian Res. 273, 67–89.

Zhu, W.G., Bai, Z.J., Zhong, H., Ye, X.T., Fan, H.P., 2017b. The origin of the c. 1.7 Ga gabbroic intrusion in the Hekou area, SW China: constraints from SIMS U–Pb zircon geochronology and elemental and Nd isotopic geochemistry. Geol. Mag. 154, 286–304.